Quaternary Science Reviews 331 (2024) 108625

Contents lists available at ScienceDirect

Quaternary Science Reviews

journal homepage: www.elsevier.com/locate/quascirev

Persistence of Holocene ice cap in northeast Svalbard aided by glacio-isostatic rebound

Wesley R. Farnsworth [a,b,c,*], Ólafur Ingólfsson [a], Skafti Brynjólfsson [d], Lis Allaart [e], Sofia E. Kjellman [c], Kurt H. Kjær [b], Nicolaj K. Larsen [b], Marc Macias-Fauria [f], Marie-Louise Siggaard-Andersen [b], Anders Schomacker [c]

[a] Nordic Volcanological Center, Institute of Earth Sciences, University of Iceland, Askja, Sturlugata 7, IS-102, Reykjavík, Iceland
[b] Globe Institute, University of Copenhagen, Øster Voldgade 5-7, DK-1350, Copenhagen K., Denmark
[c] Department of Geosciences, UiT The Arctic University of Norway, NO-9037, Tromsø, Norway
[d] The Icelandic Institute of Natural History, Borgum við Norðurslóð, IS-600, Akureyri, Iceland
[e] Near Surface Land and Marine Geology, Geological Survey of Denmark and Greenland, Universitetsbyen 81, DK-8000, Aarhus, Denmark
[f] School of Geography & the Environment, University of Oxford, Oxford, OX1 3QY, UK

ARTICLE INFO

Handling Editor: I Hendy

Keywords:
Relative sea-level change
Glacio-isostatic rebound effect
Thermophilous molluscs
Holocene thermal maximum

ABSTRACT

The deglaciation of the Svalbard-Barents Sea Ice Sheet was driven by relative sea-level rise, the incursion of North Atlantic waters around Spitsbergen, and increasing summer insolation. However, ice retreat was interrupted by asynchronous re-advances that occurred into high relative seas, during a period associated with warm regional waters and elevated summer temperatures. Better understanding of this complex style of deglaciation and the dynamic response to a warming climate can serve as an important analogue for modern warming and today's ice sheets. We present evidence from northern Svalbard of glacier re-advances during the Late Glacial-Early Holocene in hand with relative sea-level history and the occurrence of thermophilous molluscs. We argue that glacio-isostatic adjustment during the transition into the Holocene influenced ice marginal dynamics and as a result, the southern region of the Åsgardfonna ice cap persisted through the Holocene Thermal Maximum.

1. Introduction

Investigating glacier response to past warm periods allows for reconstructions of key thresholds, processes and dynamics associated with deglaciation (Jansen et al., 2020; Gowan et al., 2021; Lysså et al., 2022). These types of studies refine our current understanding and projections of glacier mass loss driven by contemporary climate change (Hugonnet et al., 2021; Geyman et al., 2022). The Arctic experiences amplified effect from these changes in climate driven by increased oceanic and atmospheric temperatures (Meredith et al., 2019; Isaksen et al., 2022; Skagseth et al., 2022). These climatic shifts lead to reduction in sea ice (Onarheim and Årthun, 2017; Detlef et al., 2023) and enhanced precipitation (Bintanja et al., 2020; Dou et al., 2022). The High Arctic archipelago of Svalbard experiences climatic changes at an even greater rate than the rest of the Arctic (Rantanen et al., 2022). Currently, the sensitive location at the northern extent of the North Atlantic Current and the southern periphery of Arctic Ocean ice is experiencing dramatic decline in glacier cover and sea-ice persistence (Noël et al., 2020; van Pelt et al., 2021; Geyman et al., 2022; Urbański and Litwicka, 2022; Efstathiou et al., 2022). The latter has a direct effect on the hydrologic regime shifting towards more frequent and often extreme precipitation events (Müller et al., 2022; Lapointe et al., 2023).

To refine our projections on the future of Arctic glaciers, we study the transition from the Late Glacial to Early Holocene (*c.* 14-8 ka BP), characterized by the deglaciation of the Svalbard-Barents Sea Ice Sheet (SBSIS) and glacier response to Svalbard's Holocene Thermal Maximum (HTM; Farnsworth and Allaart, 2024. While similar processes exist between today and the Late Pleistocene-Holocene transition (e.g., enhanced oceanic/atmospheric temperatures, sea-ice reduction, enhanced precipitation), the rate and extent of glacio-isostatic adjustment (GIA) was far greater during the deglaciation of the SBSIS than today (Forman et al., 2004).

Here we present evidence of several Late Glacial and Early Holocene glacier re-advances from outlet glaciers of the Åsgardfonna ice cap,

* Corresponding author. Nordic Volcanological Center, Institute of Earth Sciences, University of Iceland, Askja, Sturlugata 7, IS-102, Reykjavík, Iceland.
E-mail address: wesleyf@hi.is (W.R. Farnsworth).

https://doi.org/10.1016/j.quascirev.2024.108625
Received 4 December 2023; Received in revised form 26 February 2024; Accepted 18 March 2024

northeast Svalbard (Fig. 1C). Outlet glaciers advanced into the tributary fjords of Wijdefjorden, characterized by elevated Early Holocene sea-surface temperatures and regional summer warmth (Hald et al., 2004; Mangerud and Svendsen, 2018; Voldstad et al., 2020). Subsequently, it is largely believed that Svalbard glaciers retreated-back from the warm fjords, inland, to their terrestrial margins during this time (Forwick and Vorren, 2009; Bakke et al., 2018; Larsen et al., 2018). However, we highlight that some marine terminating glaciers did not retreat, but rather persisted and were subsequently glacio-isostatically uplifted from the sea after the HTM. We further provide a synthesis of geochronological constraints to the deglaciation and sea-level history of the region during the Late Glacial and Early Holocene.

1.1. Regional background

Northern Svalbard was ice-covered during the Last Glacial Maximum (LGM; Mangerud et al., 1998; Landvik et al., 1998; Ottesen et al., 2005; Ingólfsson and Landvik, 2013; Hormes et al., 2013; Hogan et al., 2017) with estimates of ice thicknesses exceeding 2 km (Patton et al., 2017; Sejrup et al., 2022). The marine sectors of the SBSIS are believed to have collapsed shortly before 14.6 cal ka BP, contributing to Meltwater Pulse 1A (Brendryen et al., 2020). This destabilization initiated wide-scale ice mass loss, which in theory resulted in accelerated *restrained rebound*, i.e., land emergence before the formation of shorelines (Wolcott, 1970; Andrews et al., 1970). Although this process has not yet been modeled

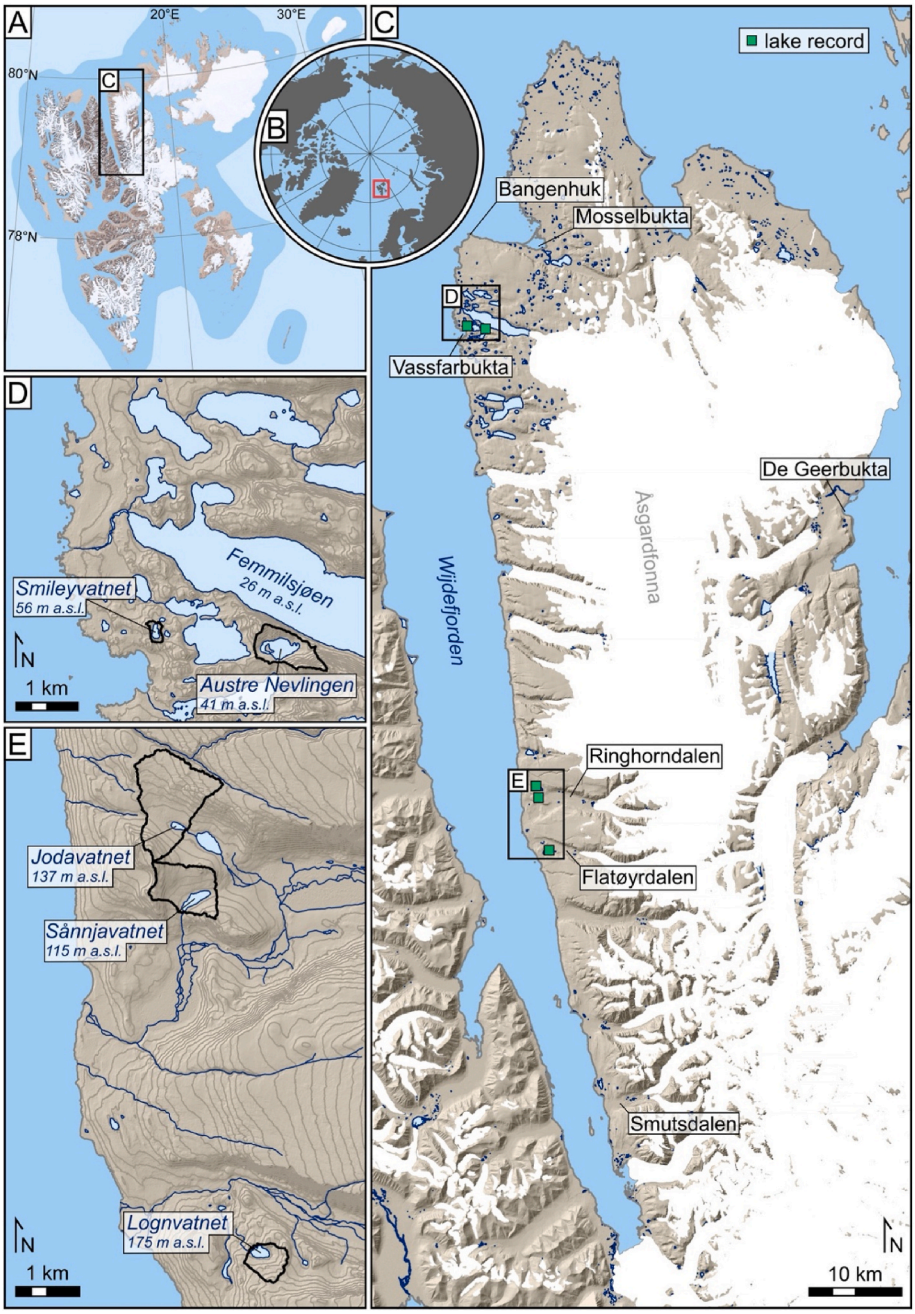

Fig. 1. A) Map of Svalbard with Wijdefjorden study region indicated. B) Overview map with Svalbard (red box) located in the Polar North Atlantic. C) Topographic map of Wijdefjorden with tributary study sites indicated (Vassfarbukta, Ringhorndalen and Flatøyrdalen), together with other place names mentioned in the text. Detailed map of the D) Vassfarbukta region and E) Ringhorndalen and Flatøyrdalen regions, with threshold lakes investigated in this study (Smileyvatnet, Sånnjavatnet, and Lognvatnet – all informal names) and previously studied lakes Austre Nevlingen (Kjellman et al., 2020), Jodavatnet (Voldstad et al., 2020) and Femmilsjøen (Allaart et al., 2021a). Black outlines indicate the lake catchments. Maps modified from Melvær (2014a, 2014b) and Norwegian Polar Institute (2017).

for Svalbard, GIA models suggest widespread land surface depression exceeding 300 m (and up to 500 m) across North America during the last deglaciation (Godbout et al., 2023). Furthermore, a similar extent of vertical bedrock motion has been estimated for the western margin of the Scandinavian Ice Sheet (Pedersen et al., 2021).

During the Late Glacial period, Wijdefjorden likely hosted an ice stream which drained a significant portion of the Svalbard component of the SBSIS (Ottesen et al., 2007; Allaart et al., 2020). While the earliest marine records at the mouth of Wijdefjorden suggest ice-free conditions between 15 and 14.5 cal ka BP (Bartels et al., 2017; Allaart et al., 2020, 2021a; Jang et al., 2023), onshore dates from shells, driftwood and whalebones suggest ice-free conditions near the fjord mouth between 14 and 12.5 cal ka BP (Salvigsen and Österholm, 1982; Mäusbacher et al., 2002; Allaart et al., 2021a). The marine limit at Bangenhuk, northeast Wijdefjorden (Fig. 1C) is estimated to 65 m a.s.l. where shells ages from the upper most (described) beach ridge date to *c.* 12.5 cal ka BP (12368-12821; see Table 1 and S1 for radiocarbon age details; Salvigsen and Österholm, 1982). The deglaciation is not well constrained throughout Wijdefjorden, however an *c.* 11.7 cal ka BP (11198-12193) shell age from the Smutsdalen tributary valley, located nearly 100 km south (Fig. 1C; close to the head of the fjord), suggests the Wijdefjorden tidewater outlet did not survive much beyond the onset of the Early Holocene (Werner, 1993; Farnsworth et al., 2020a; Allaart et al., 2021a). Two ^{10}Be exposure ages from boulders located in central Wijdefjorden date to 14.6 ± 1.0 and 13.8 ± 1.0 ka (Hormes et al., 2013), however without paired *in-situ* ^{14}C data (or ^{26}Al), the extent of inheritance remains unknown (Gjermundsen et al., 2015).

Warm Atlantic waters penetrated into Wijdefjorden during the Early Holocene, indicated by the presence of thermophilous molluscs, *Mytilus edulis* (Salvigsen, 2002; Mangerud and Svendsen, 2018). Furthermore, *sed*aDNA from the Jodavatnet lake, located in Ringhorndalen, central East Wijdefjorden (Fig. 1C and D) suggests the terrestrial realm also exhibited peak Holocene warmth during the beginning of the Early Holocene. Thus, while large portions of the Svalbard archipelago still hosted remnants of the SBSIS during the Early Holocene, ice-free regions of Wijdefjorden hosted thermophilous plant species, most of which do not occur within the fjord-system today (Eidesen et al., 2018; Voldstad et al., 2020; Farnsworth et al., 2020a).

1.2. Setting

The two study sites in northeast Svalbard, are located along the east-coast of Wijdefjorden, a 110 km long, North-South oriented fjord-system (Fig. 1). Wijdefjorden is oriented along the strike of the Billefjorden Fault Zone (Dallmann, 2015) and ranges in width from 3.3 km at the head to 25 km at the fjord mouth. A bedrock sill (at *c.* 60 m water depth) divides the fjord into an inner (southern) and outer (northern) basin, with water depths exceeding 240 and 170 m, respectively (Kowalewski et al., 1990; Allaart et al., 2020). At present four tidewater glaciers terminate into Wijdefjorden and *c.* 30 glacier-fed rivers drain into the fjord (Allaart et al., 2020). The Wijdefjorden region is characterized as relatively dry for Svalbard (Østby et al., 2017) and the glaciers exhibit some of Svalbard's greatest elevation equilibrium line altitudes (E.L.A. > 700 m; Hagen et al., 2003).

1.2.1. The Vassfarbukta bay and adjacent terrain

The Vassfarbukta bay is located at the northeast part of Wijdefjorden. The adjacent terrain to Vassfarbukta is characterized by undulating coastal lowlands consisting of widespread weathered bedrock, raised marine sediments and lake basins (Allaart et al., 2021b). The region hosts numerous isolation basins (lakes once inundated by high relative sea level; Romundset et al., 2018) and threshold lakes (basins that once received glacial meltwater; Briner et al., 2010; Schomacker et al., 2019), with Femmilsjøen being the largest (Fig. 1D; Allaart et al. 2021a, 2021b). The outlet glacier Longstaffbreen terminates into the eastern part of Femmilsjøen, draining the northwest portion of the ice cap, Åsgardfonna. Shell fragments sampled in sorted beach sediments at 65 m a.s.l. in Mosselbukta (roughly 10 km to the north of Vassfarbukta) are suggested to reflect a postglacial marine limit (Fig. 1C; Salvigsen and Österholm, 1982).

Previously published lake sediment records from the Vassfarbukta region include Austre Nevlingen, located at 41 m a.s.l. (79.783°N 15.786°E; Kjellman et al., 2020) and Femmilsjøen located at 26 m a.s.l. (79.805°N 15.732°E; Allaart et al., 2021a). Here we present one new threshold lake sediment record from Smileyvatnet (informal name; 79.786°N 15.684°E) located at 56 m a.s.l., less than 300 m from Vassfarbukta (Fig. 1C and D). At present, the Smileyvatnet catchment (*c.* 0.06 km^2) is unglaciated and without inlets or an outlet.

1.2.2. The Ringhorndalen valley and adjacent terrain

Ringhorndalen (*c.* 8 km long and 1–4.5 km wide) located near the middle of Wijdefjorden is one of the many east-west oriented tributary valleys, draining into the fjord (Fig. 1C). The two outlet glaciers Ringhornbreen and Royal Societybreen (*c.* 12 and 13.5 km long) flow from the southeastern margin of Åsgardfonna (>1200 m a.s.l.) and terminate at the head of Ringhorndalen, around 115 m a.s.l. A braided river system from the two outlet glaciers drains through bedrock, glacial sediments and raised marine deposits located in Ringhorndalen before draining into Wijdefjorden (Fig. 1C and E). Several lake basins occur in the western extent of Ringhorndalen and the Flatøyrdalen valley to the south (Fig. 1C and E). Flatøyrdalen, located *c.* 4 km south of Ringhorndalen, is also an east-west trending tributary valley. The valley extends *c.* 5.5 km from the modern coastline into the present margin of Cookbreen, which is a 1 km wide, 14 km long outlet from southern Åsgardfonna.

In addition to the published lake sediment record from Jodavatnet (Fig. 1C and E), located 137 m a.s.l. (79.3382°N 16.019°E; Voldstad et al., 2020) we present two new threshold lake sediment records. Sånnjavatnet (informal name; 79.328°N 16.031°E), located in Ringhorndalen at 115 m a.s.l., is *c.* 1 km south of Jodavatnet. Lognvatnet (informal name; 79.276°N 16.077°E) is located near the mouth of Flatøyrdalen at 175 m a.s.l. and *c.* 7 km south of Jodavatnet (Fig. 1C and E). The Sånnjavatnet (*c.* 0.30 km^2) and Lognvatnet (*c.* 0.72 km^2) catchments are relatively small compared to the Jodavatnet catchment (*c.* 1.3 km^2; Voldstad et al., 2020, Fig. 1).

2. Methods

2.1. Field investigations

Fieldwork was conducted in August 2016 (Ringhorndalen) and 2018 (Vassfarbukta) with focus on geomorphological and sedimentological mapping, as well as lithostratigraphical logging of exposed sedimentary sections. Notice was given to raised marine sediments, natural stratigraphic sections, the occurrence of shells, whalebones, and glacial landforms (Fig. 2).

Lake sediment cores were taken with a lightweight piston-corer system with 64 mm diameter coring tubes that allow for the collection of up to 200 cm long overlapping sediment cores (e.g., Voldstad et al., 2020; Kjellman et al., 2020; Allaart et al., 2021a). The coring was conducted from a small inflatable non-motorized raft. The coring was performed through a sleeve in the floor of the raft, which was anchored to obtain a stable position on the lake surface. A Hondex PS-7 Transducer LCD Digital Sounder was used for depth sounding of the lake basins. Cores were obtained from the central, deepest part of the lake basins. Duplicate cores were extracted from the lake basins and extruded (in the field) to evaluate the sediment records on site. Threshold lake catchments are generally well defined by bedrock topography and often exhibit minimum exposure to slope processes that could affect the lacustrine sedimentary record (Rubensdotter and Rosqvist, 2009). In these specific catchments, we assume minerogenic strata dominated by clay, silts and fine sand reflect a glacier signature (glacier meltwater

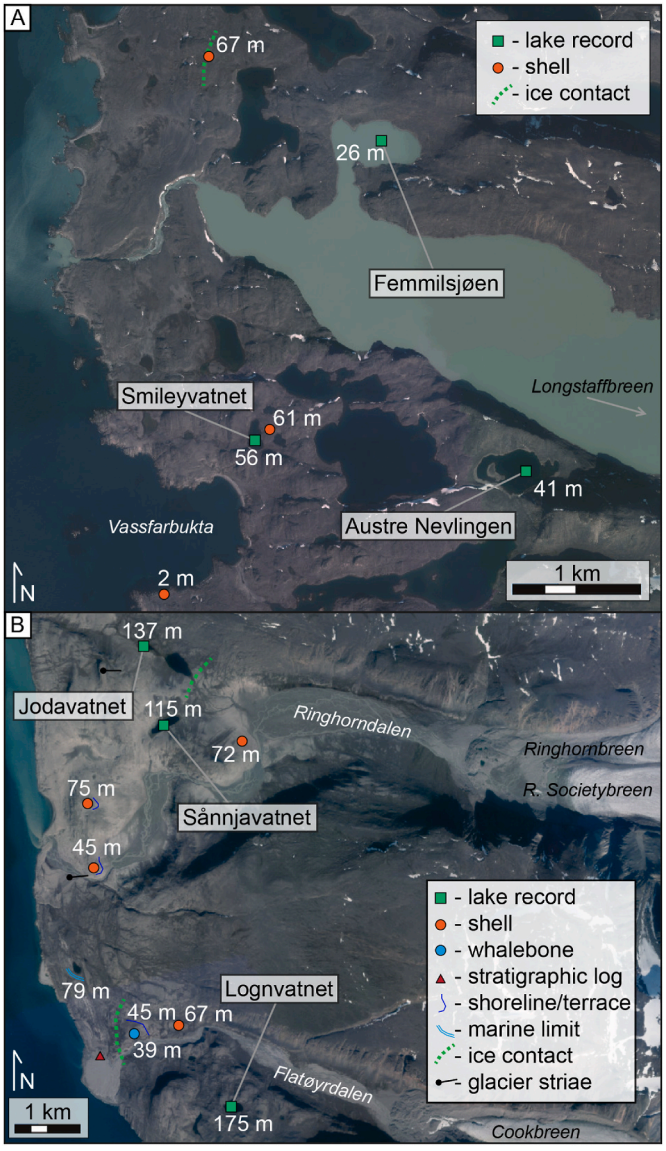

Fig. 2. Map of sampled sites with elevations for the A) Vassfarbukta and B) Ringhorndalen/Flatøyrdalen regions, eastern Wijdefjorden. Field sample elevations (±2 m uncertainty) and imagery from TopoSvalbard (https://toposvalbard.npolar.no/). N.b., lake names are informal.

reaching the lake catchment) and intervals characterized by organic rich strata (gyttja) reflect periods without glacier influence (Karlén, 1981; Briner et al., 2010; Larsen et al., 2017). Lake elevations and threshold (outlet) altitudes were measured in the field with handheld Garmin GPS as well as extracted from TopoSvalbard (The Norwegian Polar Institute). We conservatively prescribe a uniform uncertainty of ±2 m to all elevation measurements, despite overall agreement in the two techniques (Tables 1 and 2).

2.2. Chronology and laboratory analysis

To establish the glacial and relative sea level chronology, field samples (shells, driftwood, and whalebones) were cleaned, weighed, photographed and subsequently sent for radiocarbon dating. In lake sediment cores, macrofossils were sampled from residues of 0.25 and 0.5 mm sieving, isolated with tweezers and identified using a binocular microscope with tweezers. All radiocarbon ages were obtained through accelerator mass spectrometry (AMS) at the Ångström Laboratory, Uppsala University and Lund University Radiocarbon Dating Laboratory, Sweden. Ages are presented in calibrated kiloyears before present (cal. ka BP; along with their 2-sigma range) using CALIB 8.20 (Stuiver and Reimer, 1993). Terrestrial samples were calibrated using Intcal20 (Reimer et al., 2020) and marine samples were calibrated using Marine20 (Heaton et al., 2020) with a Delta R (ΔR) of −61 ± 37 for shells and ΔR = −160 ± 41 for whalebones (Pieńkowski et al., 2022). We present new radiocarbon constraints in figures as median values, rounded up to the nearest century. Ages referred to in text are followed by their 2-sigma range. All geochronological details are included in Tables 1, 2 and S1. Metadata are presented in accordance with recent database standard (e.g. Hughes et al., 2016; Farnsworth et al., 2020a). Previous studies and radiocarbon dates from the area are referenced and re-calibrated accordingly, to better constrain the glacial history of the fjord (Table S1).

Lake sediment cores were split open, logged and analyzed in the sediment lab and ITRAX core facility at the Centre for GeoGenetics, Globe Institute, University of Copenhagen. The lithology and stratigraphy of the cores were visually inspected and logged. ITRAX scanning was run on each of the sediment cores to record visual and radiographic imagery, magnetic susceptibility, and X-ray fluorescence (XRF; Kylander et al., 2011).

3. Results

Nineteen new radiocarbon ages from shells, whalebone, driftwood and macrofossils (from lake sediments) are presented from the Vassfarbukta and Ringhorndalen regions (Fig. 2; Tables 1 and 2). Sample locations and respective elevations (data extracted from TopoSvalbard, The Norwegian Polar Institute) are presented for both regions (Fig. 2). Elevations correspond to sample site and lake surface elevation. Details associated with radiocarbon ages and elevation uncertainty (±2 m) are presented in Tables 1 and 2

3.1. Vassfarbukta regional radiocarbon chronology

Samples were collected from three distinct locations in the Vassfarbukta region (Fig. 2). The northernmost sample site is a prominent *c.* 2.5 m tall, N–S oriented ridge crest (67 m a.s.l.), composed of unsorted sediments and reworked shells (Fig. 3A and B). A radiocarbon dated shell fragment (Ua-61453) collected from the diamict suggests the ridge was deposited after *c.* 13.0 cal ka BP (12793-13158; Table 1). Furthermore, the shell-bearing ridge is interpreted as an ice-marginal deposit resulting from a glacier re-advancing into the sea (which was somewhat below 67 m a.s.l.; Fig. 3A and B). The second Vassfarbukta sample site is located 45 m east of Smileyvatnet at 61 m a.s.l. At this site, a reworked shell fragment (*Hiatella arctica;* Ua-73898) was sampled from a cryoturbated diamict on the top of the bedrock knob above the lake. This age constrains the initial deglaciation of the land around Vassfarbukta to *c.* 13.5 cal ka BP (13292-13718). The southern sample site from the Vassfarbukta region is a coastal section (*c.* 0–1.5 m a.s.l.) exposed on the southern shore of Vassfarbukta. The high section is composed of gravels and cobbles with outsized boulders (Figs. 2 and 3C). The section includes outcropping driftwood logs (Ua-73899) and blue mussel shells (*Mytilus edulis;* Ua-73897). Both radiocarbon ages yield Middle Holocene ages, respectively *c.* 7.3 and *c.* 7.1 cal ka BP (7267–7422; 6891–7259; Fig. 3C; Table 1).

3.2. Ringhorndalen and Flatøyrdalen regional chronology

Shells were collected from wave-washed terraces located at 75 m a.s.l. and 45 m a.s.l. (Figs. 2, 3D and 3E). Reworked shell fragments were dated from both features exhibiting *c.* 11.6 and *c.* 10.2 cal ka BP, respectively (11307-11867; 10035-10482). This data builds on a previous investigation from Sharin et al. (2007) which describes raised marine sediments (often morphologically expressed as raised beaches) in the Ringhorndalen region exceeding 30 m a.s.l. The highest raised

Table 1
Radiocarbon ages of field samples from Vassfarbukta (VFB), Ringhorndalen (RHD), and Flatøyrdalen (FØD), calibrated with CALIB 8.20 (Stuiver and Reimer, 1993) Marine samples have been re-calibrated with Marine20 (Heaton et al., 2020) using a ΔR of −61 ± 37 for shells and −160 ± 41 for whalebone (Pieńkowski et al., 2022). Terrestrial samples calibrated with Intcal20 (Reimer et al., 2020). Median ages in **bold.**

Region	Sample material	Elev. (m)	Sample ID	Latitude & Longitude	Sample & medium	^{14}C age (yr BP)	Median age (cal. yr BP)	Age range 2σ (cal. yr BP)
VFB	shell fragment	61 ± 2	Ua-73898	79.7855°N 15.6880°E	VFB-14 shell bearing diamict	12095 ± 57	**13489**	13292-13718
VFB	shell fragment	67 ± 2	Ua-61453	79.8113°N 15.6695°E	VFB-20 shell bearing diamict	11606 ± 49	**12986**	12793-13158
VFB	blue shell fragment	2 ± 2	Ua-73897	79.7749°N 15.6449°E	VFB-01 in coastal section	6713 ± 38	**7083**	6891–7259
VFB	driftwood	2 ± 2	Ua-73899	79.7749°N 15.6438°E	VFB-12 in coastal section	6412 ± 35	**7342**	7267–7422
RHD	shell fragment	75 ± 2	LuS-10804	79.3174°N 15.9775°E	terrace-topped sands & gravels	10460 ± 55	**11595**	11307-11867
RHD	shell fragment	45 ± 2	LuS-10803	79.3082°N 15.9817°E	terrace-topped sands & gravels	9480 ± 50	**10243**	10035-10482
RHD	shell fragment	70 ± 2	LuS-10809	79.3231°N 16.0977°E	shell bearing diamict	9390 ± 50	**10123**	9881–10338
RHD	shell fragment	1 ± 1	Ua-62169	79.3043°N 15.9384°E	coast cut diamict	8012 ± 35	**8371**	8197–8534
RHD	driftwood	9 ± 2	Ua-56092	79.3065°N 15.9402°E	driftwood in beach ridge	1220 ± 27	**1137**	1064–1259
RHD	driftwood	4 ± 2	Ua-56091	79.2840°N 15.9749°E	driftwood in beach ridge	185 ± 26	**183**	0–295
FØD	shell fragment	68 ± 2	LuS-10806	79.2872°N 16.0436°E	shell bearing diamict	10185 ± 55	**11210**	10995-11476
FØD	shell fragment	11 ± 2	LuS-10807	79.2833°N 15.9938°E	*Mya truncata* clay-silt, section	10290 ± 55	**11348**	11140-11626
FØD	whalebone	39 ± 2	LuS-10805	79.2863°N 16.0082°E	raised beach	9805 ± 55	**10838**	10576-11091
FØD	paired shell	14 ± 2	Ua-56090	79.2833°N 15.9938°E	*Mya truncata* sand section	9663 ± 40	**10469**	10247-10673
FØD	shell fragment	15 ± 2	LuS-10808	79.2833°N 15.9938°E	*Mytilus edulis* gravel section	9615 ± 50	**10406**	10204-10628

Table 2
Radiocarbon ages of macrofossils from lake sediment cores from Vassfarbukta (VFB), Ringhorndalen (RHD), and Flatøyrdalen (FØD) compared to previous lake studies (Jodavatnet; Voldstad et al., 2020; Austre Nevlingen; Kjellman et al., 2020; Femmilsjøen; Allaart et al. 2021a). All ages calibrated with CALIB 8.20 (Stuiver and Reimer, 1993) using IntCal20 (Reimer et al., 2020).

Lake/Region	Sample material	Elev. (m)	Sample ID	Latitude & Longitude	Sample & interval	^{14}C age (yr BP)	Median age (cal. yr BP)	Age range 2σ (cal. yr BP)	Reference
Smileyvatnet, VFB	aquatic bryophyte	56 ± 2	Ua-74819	79.7857°N 15.6831°E	Smiley18 SPB_27-28	10175 ± 41	**11833**	11644-11962	This study
Smileyvatnet, VFB	aquatic bryophyte	56 ± 2	Ua-74820	79.7857°N 15.6831°E	Smiley18 SPB_30–30.5	10632 ± 45	**12667**	12499-12727	This study
Sånnjavatnet, RHD	aquatic bryophyte	115 ± 2	Ua-55371	79.328°N 16.0310°E	Sannja16 SVP1_101-102	7819 ± 44	**8594**	8454–8762	This study
Lognvatnet, FØD	aquatic bryophyte	175 ± 2	Ua-55370	79.276°N 16.077°E	Logn16 LVP2A_109-110	9880 ± 37	**11272**	11211-11394	This study
Lognvatnet, FØD	unidentified plant detritus	175 ± 2	Ua-55372	79.276°N 16.077°E	Logn16 LVP2B_0–0.5	12238 ± 47	**14151**	14043-14769	This study
Jodavatnet, RHD	terr. plant macrofossil	137	Ua-55365	79.3382°N 16.019°E	Joda16 JVP_177-178	9512 ± 40	**10807**	10589–11073	Voldstad et al. (2020)
Jodavatnet, RHD	aquatic bryophyte	137	Ua-55366	79.3382°N 16.019°E	Joda16 JVP_185-186	10426 ± 42	**12308**	12060–12604	Voldstad et al. (2020)
Austre Nevlingen, VFB	aquatic bryophyte	41	LuS 12221	79.7839°N 15.7866°E	AustreNev15 ANP3_95.5–96.5	10070 ± 75	**11603**	11282-11877	Kjellman et al. (2020)
Femmilsjøen, VFB	aquatic bryophyte	26	Ua-64442	79.805°N 15.732°E	Femmil18 FMP1_72-73	8705 ± 43	**9649**	9543–9888	Allaart et al. 2021a,
Femmilsjøen, VFB	aquatic algae *Phaeophyceae*	26	Ua-64451	79.805°N 15.732°E	Femmil18 FMP3_28-29	10469 ± 75	**11409**	11203–11650	Allaart et al. 2021a,

beach sediments we identify in the region extend up to 79 m a.s.l between Ringhorndalen and Flatøyrdalen (Fig. 2), however lack radiocarbon constraint.

We suggest the uppermost beach ridge corresponds to the postglacial sea level shortly after the regional deglaciation, before *c.* 11.6 cal ka BP (11307-11867). Shell fragments resedimented in diamict (and not reflecting shoreline age) at 72 m a.s.l. (Ringhorndalen) and at 67 m a.s.l. (Flatøyrdalen) date to *c.* 10.1 and *c.* 11.2 cal ka BP, respectively (9881–10338; 10995-11476; Fig. 2). Furthermore, a whale cranium (ear bone) was sampled on a wave-washed terrace at 39 m a.s.l. (under a 45 m a.s.l. shoreline), yielding an age of *c.* 10.8 cal ka BP (10576-11091; Figs. 2 and 3E). Despite abundant driftwood on modern Ringhorndalen beaches from the last 500 years (Hole et al., 2021), minimal driftwood was encountered on the raised beaches in the area. However, two driftwood samples, collected at 9 and 4 m a.s.l., date to *c.* 1.1 cal ka BP (1064–1259) and modern, respectively (Table 1).

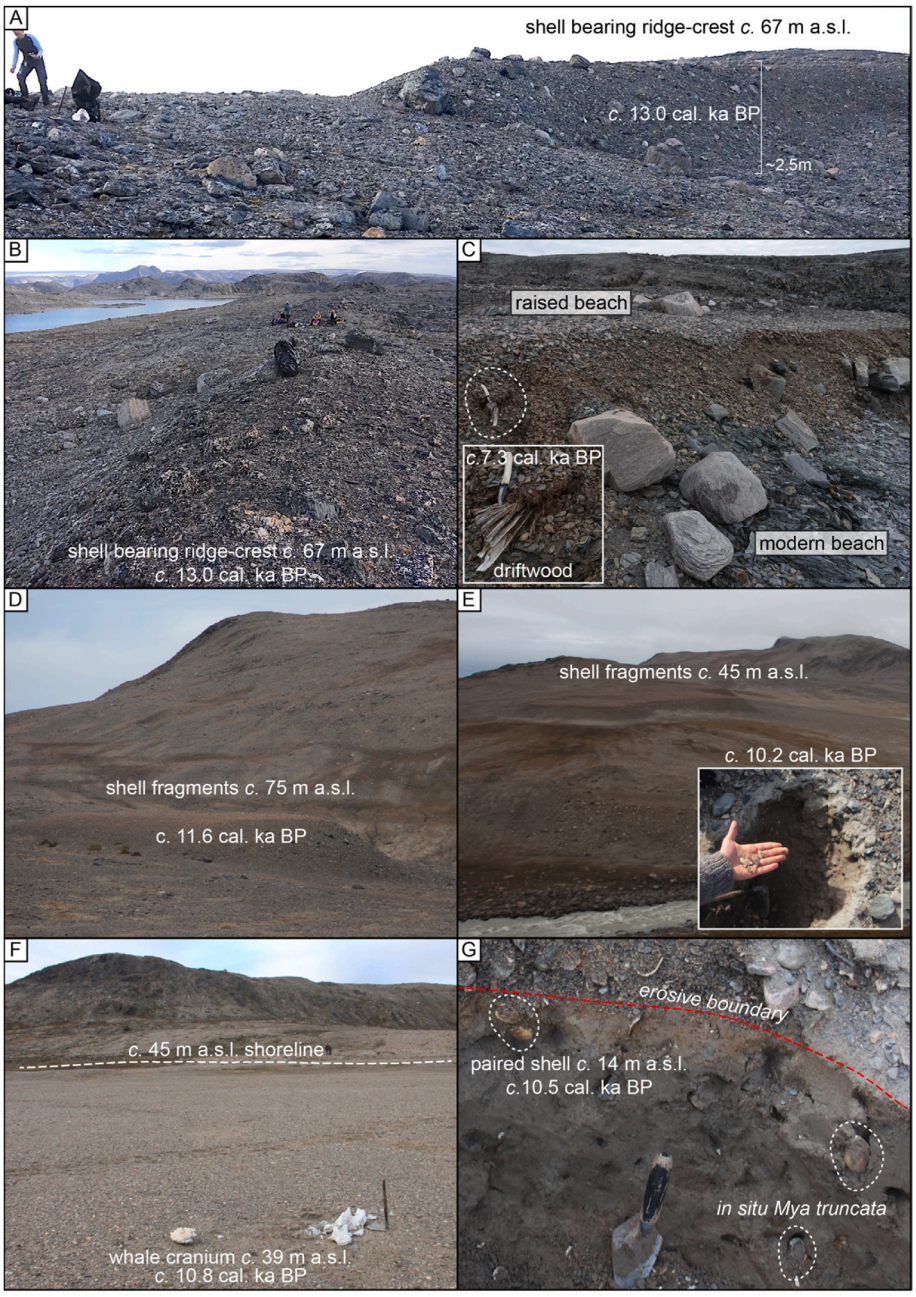

Fig. 3. Photomosaic of investigated landforms and selected field sample locations in Vassfarbukta (A, B and C); Ringhorndalen (D and E); and Flatøyrdalen (F and G). Sample elevation and calibrated radiocarbon ages (cal. ka BP) indicated. Radiocarbon age details listed in Table 1.

At the mouth of Flatøyrdalen (north of the river), a natural section was cleared, lithostratigraphically logged and sampled for radiocarbon dating (Figs. 2, 3G and 4). Three radiocarbon dates constrain the sequence reflecting deglaciation and Early Holocene glacial sedimentation. The location appears to have become ice-free before *c.* 11.4 cal ka BP (11140-11626), constrained by a *Mya truncata* fragment from within the clayey silt near the section base (Fig. 4; Table 1). The section displays a coarsening upwards (regressional) sediment sequence, common around Svalbard, suggestive of shallowing marine conditions during rapid postglacial uplift (Mangerud and Svendsen, 1992; Ingólfsson et al., 1995; Alexanderson et al., 2018). A crudely sorted, clast rich, sandy gravel (containing shell fragments, cobbles, and boulders) interrupts the coarsening upwards sequence around *c.* 10.4 cal ka BP (10204-10628). This bed contains the thermophilous mollusc *Mytilus edulis*.

3.3. Threshold lake lithostratigraphy

Stratigraphy from three lake sediment records is characterized by two different lithofacies (LF-1 and LF-2; Figs. 2 and 5). In the following sections, threshold lake sediment records and constraining geochronology are presented from Vassfarbukta (Smileyvatnet) and subsequently the Ringhorndalen region (Sånnjavatnet and Lognvatnet). We further compare new records to three previously published records from the region including Jodavatnet (Voldstad et al., 2020), Austre Nevlingen (Kjellman et al., 2020) and Femmilsjøen (Allaart et al. 2021a). We implement our lithofacies according to previously published sediment descriptions and refer to previously published ages (Table S1). At present, all lake catchments are ice-free, located three to six km from the most proximal ice margin except Femmilsjøen which remains proglacial (Longstaffbreen terminates in the eastern margin of the lake).

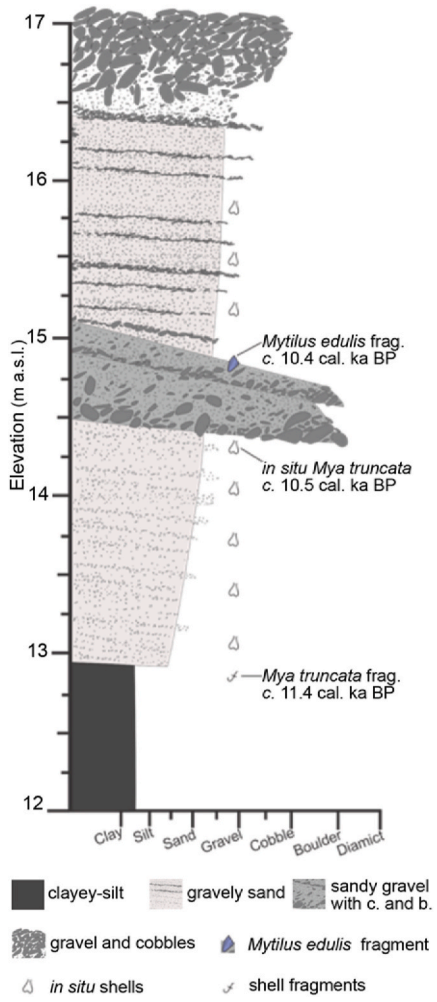

Fig. 4. Schematic lithostratigraphic log of the river section at the mouth of the Flatøyrdalen valley presented with calibrated radiocarbon ages. N.b., the regressional sequence is interrupted by an interval of sandy gravel with cobbles, boulders and shell fragments. Radiocarbon age details can be found in Table 1.

3.3.1. *Smileyvatnet – 56 m a.s.l.*

Two overlapping piston cores were collected in the basin of Smileyvatnet at *c.* 6.5 m water depth. Recovered composite stratigraphy is estimated to *c.* 185 cm based on coring measurements. Here we present ITRAX scan data from the lowermost *c.* 79 cm of strata (Fig. 5A). Due to the poor preservation of the overlaying strata, lake sediments from 107 to 0 cm were not scanned or investigated. Changes in the depositional environment are revealed based on variations in lithology, geochemical composition and organic content (Fig. 5A). The lowermost stratum of the Smileyvatnet record is divided into two lithofacies.

Lithofacies 1 (LF-1) covers the lowermost 48 cm of composite strata, from 184 to 137 cm. LF-1 consists of reddish grey clayey-silty diamict with crudely laminated to laminated strata interrupted by outsized gravel clasts (especially from 185 to 170 cm). The combination of a darkened radiogram, elevated magnetic susceptibility (MS) values and titanium (Ti) reads indicate minerogenic-rich sediments with minimal organic material. We interpret LF-1 as deposited by glacial meltwater draining into the Smileyvatnet catchment. Our LF-1 is consistent with the lowermost stratum from Austre Nevlingen (L1; Kjellman et al., 2020) and Jodavatnet (LU 1; Voldstad et al., 2020).

Lithofacies 2 (LF-2) spans the overlaying 31 cm of strata from *c.* 137-106 cm in the composite core. LF-2 consists of dark brown to brown laminated gyttja with occasionally interbedded silt beds. LF-2 exhibits reduced indicators of glacially derived minerogenic sedimentation (MS, X-ray derived density and Ti) and is characterized by organic rich strata and gyttja accumulation. We interpret LF-2 as predominantly biogenetic accumulation deposited within the lake during periods without inflow of glacial meltwater (e.g., Kaplan et al., 2002; Briner et al., 2010; Larsen et al., 2015). The transition from LF-1 to LF-2 is sharp, pronounced in the optical image, radiogram and ITRAX data (Fig. 5A). Two macrofossils (aquatic bryophytes) have been radiocarbon dated from the lowermost strata in LF-2 (at 27–28 cm and 30–30.5 cm; *c.* 131–132 cm and 136–136.5 cm composite record) from the Smileyvatnet sequence. The ages suggest the transition from LF-1 to LF-2 occurred *c.* 12.7 cal ka BP (12499-12727; Table 2).

3.3.2. *Sånnjavatnet – 115 m a.s.l.*

A piston core was collected from the main basin of Sånnjavatnet at *c.* 16 m water depth (Figs. 2 and 5B). The *c.* 151 cm long core is classified into the two lithofacies, LF-1 and LF-2 (Fig. 5). The lowermost 48 cm (*c.* 151-103 composite stratigraphy) is classified as LF-1 (Fig. 5B). The sediments are tan to olive grey, laminated silts and sands characterized by a dense (dark) radiograph and elevated MS and Ti reads (Fig. 5B). Despite the color and the slightly coarser nature, LF-1 from Sånnjavatnet is comparable to LF-1 from Smileyvatnet and is also suggested to reflect minerogenic-rich sedimentation derived from glacial meltwater entering the catchment (e.g., Briner et al., 2010; Larsen et al., 2015).

Lithofacies 2 (LF-2) in Sånnjavatnet makes up the overlying 103 cm of strata (Fig. 5B), following a sharp transition from LF-1. Lithofacies-2 consists of light brown to tan-brown laminated gyttja, occasionally interbedded with silts or fine sands. Sedimentological characteristics exhibit reduced radiographic signal, as well as low MS and Ti reads. This is consistent with LF-2 from Smileyvatnet, Austre Nevlingen and Femmilsjøen (L1; Kjellman et al., 2020; LF-4 Allaart et al., 2021a) to the north and the proximal Jodavatnet (LU 1; Voldstad et al., 2020, Fig. 5B, D-F). Like previous studies, we interpret these characteristics to reflect biogenic sediment accumulation in a glacier-free catchment. A single aquatic macrofossil (aquatic bryophyte) was sieved from the Sånnjavatnet record at 101–102 cm, near the bottom of LF-2 (Table 2). The calibrated age suggests a transition from LF-1 to LF-2 shortly before *c.* 8.6 cal ka BP (8454–8762).

3.3.3. *Lognvatnet – 175 m a.s.l.*

A piston core was collected from the main basin of Lognvatnet at *c.* 9.5 m water depth (Figs. 2 and 5C). The core is *c.* 140 cm long (Fig. 5C) and has been divided into lithofacies 1 and 2 (LF-1 and LF-2). We classify the lowermost 28 cm (*c.* 140 to 112 cm composite stratigraphy) as LF-1 characterized as bedded to massive, tan grey to light olive silt and fine sand. The sediment sequence exhibits elevated MS and Ti reads as well as a dense radiograph signal, suggestive of minerogenic glaciofluvial sedimentation (i.e., glacial meltwater) into the lake catchment.

The uppermost 112 cm is characterized as LF-2. The crudely bedded tan-brown to dark brown gyttja increases in organic material upwards. The elevated organic content in hand with the low MS, Ti reads and reduced radiograph density is suggestive of a catchment free of glacial meltwater. Two centimeters above the sharp boundary between LF-1 and LF-2, an aquatic bryophyte (109–110 cm), dates to *c.* 11.3 cal ka BP (11211-11394). Furthermore, organic detritus sampled from the top of LF-1 (111–112 cm) dates to *c.* 14.2 cal ka BP (14043-14769). Although the present catchment does not consist of bedrock containing old carbonates, the Polheim and Rittervatnet units from the Atomfjella Complex, east of Lognvatnet contain marble (Dallmann, 2015). Given that LF-1 has what we interpret as glacial meltwater sedimentation, we cannot rule out the incorporation of older carbon exaggerating the age of the un-identified macrofossils. Given the macrofossils are not terrestrial, the glacially influenced extended catchment and the potential of old carbon entering the lake system, we do not consider the lowermost organic detritus radiocarbon age from LF-1 reliable.

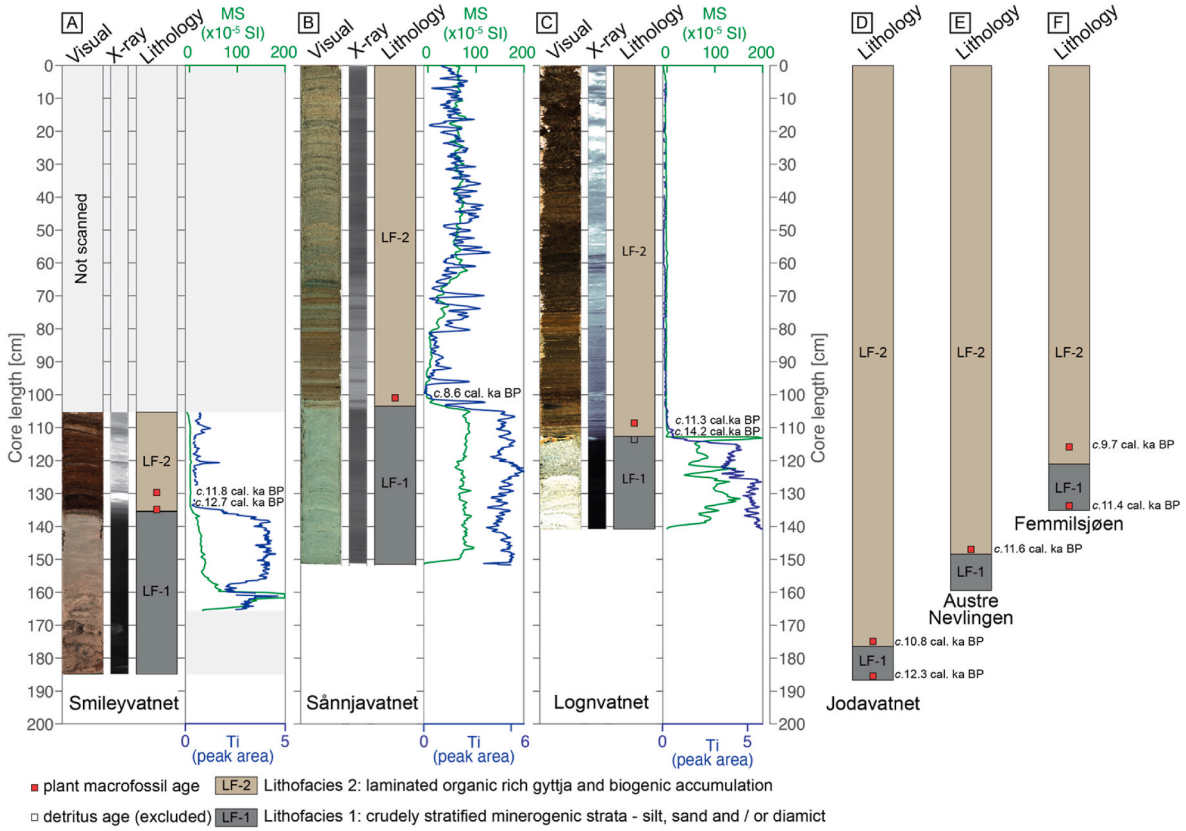

Fig. 5. Stratigraphic data (visual, radiograph, sedimentological log, magnetic susceptibility (MS), normalized Ti and calibrated radiocarbon ages) from lakes A) Smileyvatnet, Vassfarbukta; B) Sånnjavatnet, Ringhorndalen and C) Lognvatnet, Flatøyrdalen. D-F) Simplified stratigraphic logs with lithofacies for Jodavatnet, Ringhorndalen; Austre Nevlingen and Femmilsjøen, Vassfarbukta (Voldstad et al., 2020; Kjellman et al., 2020; *in review;* Allaart et al., 2021a). Radiocarbon age details are listed in Table 2.

4. Discussion

4.1. Regional deglaciation, ice-marginal constraints and sea-level history

In the following sections we reconstruct a series of events associated with the Late Glacial and Early Holocene deglaciation, ice-marginal fluctuations and sea-level history for Vassfarbukta as well as for Ringhorndalen-Flatøyrdalen. We find these events to be the simplest solution to the mosaic of evidence collected.

4.1.1. Vassfarbukta

A marine core taken *c.* 5 km north of Vassfarbukta suggests the site was deglaciated before *c.* 12.4 cal ka BP (Allaart et al., 2020). The earliest age constraint we present suggests ice-free conditions 0.5 km inland from Vassfarbukta by *c.* 13.5 cal ka BP (13292-13718; east of lake Smileyvatnet; Fig. 2A). This extends the terrestrial deglaciation age from Bangenhuk of *c.* 12.5 cal ka BP (12368-12821) by 1 ka (Table S3; Salvigsen and Österholm, 1982). Field data suggests a minor ice marginal re-advance occurred after *c.* 13.0 cal ka BP (12793-13158) into the fjord when relative sea level was likely located just beneath 67 m above present (Fig.. 2A and 3A and B). The ice margin formed the sub-aerial shell-bearing ridge crest located between Femmilsjøen and Gunvorvatnet *c.* 1 km from the present coast. The lowermost macrofossil age from the Smileyvatnet lake sediment record (constraining the boundary between LF-1 and LF-2) suggests the ice margin had abandoned the ridge crest and retreated to the east of the lake catchment by *c.* 12.7 cal ka BP (12499-12727; Fig. 6). We assume this minor fluctuation of the Longstaffbreen outlet glacier occurred between *c.* 13–12.7 cal ka BP coinciding with the end of the Allerød and onset of the Younger Dryas chronozone. Given the proximity of the moraine ridge crest (*c.* 0.9 km

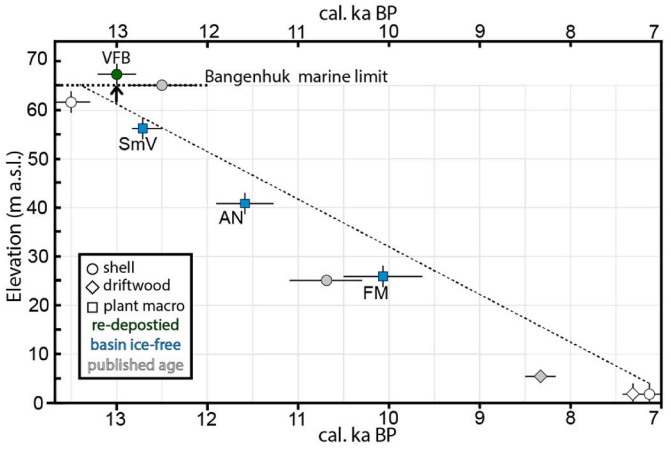

Fig. 6. Constraints on postglacial sea level for the Vassfarbukta region. Radiocarbon ages from shells (circles), driftwood (diamonds) and plant-macro fossils from isolation basins (squares) reflect mean sea level and ice-free conditions. The shell located at 67 m a.s.l. (green) was re-deposited above the marine limit by a Late Glacial re-advance from Longstaffbreen (VFB = Vassfarbukta). Radiocarbon ages from Bangenhuk raised beaches indicated by grey color and marine limit is indicated by a dotted line (Salvigsen and Österholm, 1982). Threshold lake basin deglaciations are indicated in blue squares (SmV = Smileyvatnet; AN = Austre Nevlingen; Kjellman et al., 2020; FM = Femmilsjøen; Allaart et al., 2021a).

north) and Smileyvatnet lake (*c.* 1 km south) to the Femmilsjøen basin, we assume uniform behavior of the Longstaffbreen outlet and peripheral ice margin in our interpretation of this re-advance. The deglaciation of the outlet glacier is further constrained by the *c.* 11.6 cal ka BP (11282-11877) basal age of Austre Nevlingen sediment sequence roughly 2.5 km further east (Fig. 6; Kjellman et al., 2020). This is in accordance with the *c.* 11.4 cal ka BP (11203–11650) macrofossil age from the north basin of Femmilsjøen (Fig. 2A; Allaart et al. 2021a). We follow the SVALHOLA database quality standards and consider bulk sediment ages to be of the lowest constraining value (Farnsworth et al., 2020a). Accordingly, we only discuss macrofossil ages from the lake sediment records (even though the Strøen bulk ages from Hyvärinen (1970) fit within the deglaciation interval, albeit with large uncertainty).

Sedimentological analysis from the Femmilsjøen north basin suggests a reduction in minerogenic inflow to the core site *c.* 10.1 cal ka BP, interpreted as a greatly reduced Åsgardfonna ice cap (Allaart et al., 2021a). Shell and driftwood ages (*c.* 7.1 and *c.* 7.3 cal ka BP respectively; 6891–7259; 7267–7422) from the Vassfarbukta coast (2 m a.s.l.) align with relative sea-level data from Bangenhuk (Salvigsen and Österholm, 1982) as well as the presence of *Mytilus edulis* within the fjord during the Early and Middle Holocene (Salvigsen, 2002; Mangerud and Svendsen, 2018). Sparse evidence of Middle and Late Holocene driftwood and pumice could indicate that sea level dropped below modern conditions during the Middle Holocene and only during the last centuries transgressed to its present level (Salvigsen and Österholm, 1982; Farnsworth et al., 2020b; Allaart et al. 2021a; Hole et al., 2021). Further investigations of sea-level history, isolation basins and the shallow marine environment are needed to better constrain this interval in Svalbard's Holocene relative sea level history.

4.1.2. Ringhorndalen

It remains unclear when the Wijdefjorden glacier and Ringhorndalen outlet disconnected. However, the Jodavatnet basal age suggests the basin had established prior to *c.* 12.3 cal ka BP (12060−12604; albeit held glacial inflow until *c.* 10.8 cal ka BP; 10589−11073). Presumably, the basal age is roughly the age of the 79 m a.s.l. marine limit, located to the south of the mouth of Ringhorndalen (Fig. 2B). The relative sea level is constrained by two terraces located at 75 and 45 m a.s.l. (Fig. 2B). Both terraces contain shells dating to *c.* 11.6 and *c.* 10.2 cal ka BP (11307-11867; 10035-10482), respectively and are interpreted to represent the sea level at the time of formation.

Following deglaciation of the Jodavatnet basin, both Jodavatnet and the unnamed lake to the east were likely one contiguous body of water with two sub-basins (Fig. 7A). The elevated lake level was supported by a damming ice margin to the east, forcing meltwater through a spillway (S^1 at *c.* 156 m a.s.l.) draining to the west (Fig. 7A). This configuration likely persisted until *c.* 10.8 cal ka BP, when the Ringhorndalen ice margin retreated from the palaeo-lake and the drainage re-routes to a more easterly spillway (S^2) cutting through the former Early Holocene (EH^1) ice margin. At this time, we assume the Jodavatnet lake basin ceased to receive glacial meltwater (transitions to LF-2), the lake level dropped from 156 to 137 m a.s.l. and the palaeo-lake divided into two basins separated by a roughly 175 m wide straight. The eastern lake level dropped to 134 m a.s.l. as the eastward spillway (S^2) incised through the glacial sediments (Fig. 7B).

The Ringhorndalen outlet glacier retreated from the palaeo-lake to an unknown extent *c.* 10.8 cal ka BP (10589−11073; EH^2; Fig. 7B). During this time, molluscs colonized the shallow fjord, only to become incorporated into glacial sediments during a re-advance after *c.* 10.1 cal ka BP (9881–10338). The ice margin re-advanced to the Sånnjavatnet lake basin (EH^3), just shy of its initial position (EH^1; Fig. 7C). The maximum extent of the re-advance can be indirectly inferred from the

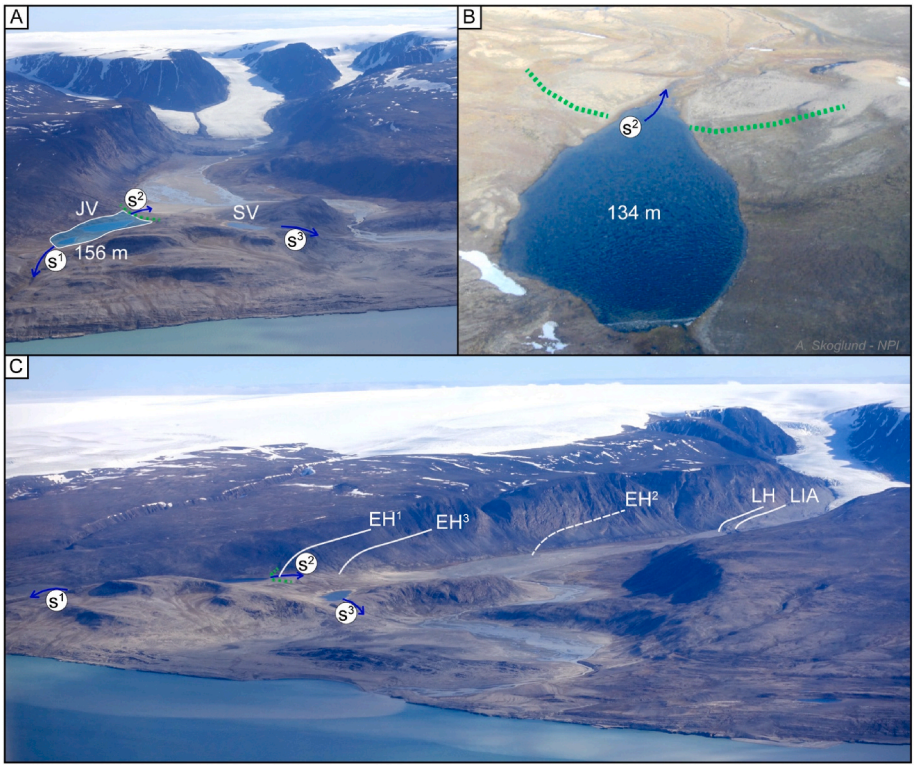

Fig. 7. Photomosaic of oblique aerial images of the mouth of Ringhorndalen. A) overview of the palaeo-lake Jodavatnet (JV), dammed to the west by the Early Holocene (EH^1) Ringhorndalen outlet glacier. Spillway 1 (S^1) draining to the west through a 156 m a.s.l. threshold. B) View of the ice marginal glacier deposit derived from the lake-damming Ringhorndalen outlet, subsequently incised by the second spillway (S^2). C) Overview of the three spillways S^{1-3} and the schematic corresponding ice margins EH^{1-3}. Note that spillway 3 (S^3) drains to the southwest through Sånnjavatnet (SV). Schematic Late Holocene (LH), Little Ice Age (LIA) profiles indicated (in white) and modern margin visible for relative comparison.

Jodavatnet stratigraphy. The uninterrupted accumulation of gyttja during this time interval, devoid of minerogenic glacial fingerprinting, suggests the margin did not return fully to its previous extent (EH^1). Following the re-advance, a third spillway was established, where meltwater drained through Sånnjavatnet, to the south (S^3; Fig. 7C). This drainage persisted until shortly before *c.* 8.6 cal ka BP (8454–8762), when the Sånnjavatnet sediment record transitioned from LF-1 to LF-2, indicating no more glacial meltwater inflow.

The Jodavatnet record does not contain a glacial diamict at its base (Voldstad et al., 2020). It thus remains unclear if the Ringhorndalen outlet glacier retreated completely out of the Jodavatnet catchment prior to the lake basal age (suggesting the EH^1 ice margin relates to an earlier re-advance, prior to *c.* 12.3 cal ka BP; 12060−12604). To our knowledge, this is the first evidence of a Svalbard glacier persisting as a tidewater margin, only to be uplifted out of the marine realm due to GIA.

4.1.3. Flatøyrdalen

The Flatøyrdalen deglaciation seemingly occurred after the Ringhorndalen deglaciation, constrained by the base of the Lognvatnet lake sediment record, as well as the base of the lithostratigraphic section located at the valley mouth (*c.* 11.3 and *c.* 11.4 cal ka BP, respectively 11211-11394; 11140-11626). Like Ringhorndalen, the Flatøyrdalen outlet glacier, Cookbreen, also re-advanced during the Early Holocene. Evidence for the ice marginal fluctuation is built upon a combination of spatial and stratigraphic factors. This included the stratigraphic section at the valley mouth, the ice contact (east of the section), a whale cranium at 39 m, beneath a 45-m shoreline (east of the ice margin; Figs. 2, 3F and 3G) and a shell bearing diamict above the 45-m shoreline. No raised beaches above 45 m a.s.l. are found in Flatøyrdalen, (east of the ice contact). Above the 45-m shoreline (and to the east of the ice contact) shell bearing diamict is widespread. A shell fragment collected from within the diamict at 67 m a.s.l. (roughly 1 km east of the whale cranium) dates to *c.* 11.2 cal ka BP (10995-11476). During the re-advance, the outlet glacier also reworked the whale cranium, *c.* 10.8 cal ka BP (10576-11091), redepositing it down to 39 m a.s.l., roughly 20–25 m beneath the projected relative sea level of its age. While the ice margin did not overrun the lithostratigraphic section at the mouth of the valley, it likely extended to within a couple of hundred meters (of the section) at its maximum (Fig. 2; given the re-sedimentation of the whale cranium <0.5 km to the east of the section). However, based on the stratigraphic section (located outboard of the ice margin) with an outsized, clast-rich bed of cobbles and gravels (largely devoid of fines) interrupting a sandy regressional sequence, we suggest the re-advance occurred *c.* 10.4 cal ka BP (Fig. 4). We interpret this as ice proximal, high-energy sedimentation (e.g. glacial debris lobe), not a subglacial deposit. The combination of *in situ* paired shells stratigraphically beneath the diamict (Fig. 3G) and the *Mytilus edulis* located in the top of the unit dating to *c.* 10.5 and *c.* 10.4 cal ka BP (respectively,10247–10673; 10204-10628), suggests the advance was likely short lived. Given the resedimented whalebone was deposited on a terrace corresponding to a 45 m a.s.l. shoreline (Figs. 2 and 3F), we can infer the ice margin had started to retreat from its maximum extent by *c.* 10.2 cal ka BP (10035-10482; if we utilize the age of the 45 m a.s.l. terrace from Ringhorndalen, located 2.5 km to the north of the 45-m shoreline). Additionally, the outlet re-advance was topographically well constrained and likely exhibited a gentle surface profile as no glacial meltwater entered the Lognvatnet catchment located at 175 m a.s.l. We can compile the Ringhorndalen–Flatøyrdalen regional data into one plot constraining Early Holocene relative sea level and displaying where marine fauna was redeposited by glacier fluctuations (Fig. 8).

4.2. Dynamic Åsgardfonna outlet glaciers and the Holocene glacial minimum

We identify a series of asynchronous glacier re-advances occurring during a period associated with deglaciation (Fig. 9). Palaeoclimatic

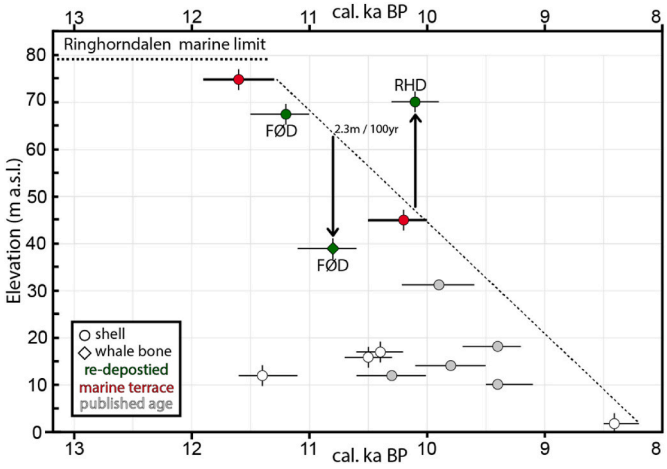

Fig. 8. Relative sea-level minimum constraints for the Ringhorndalen region. Radiocarbon ages from shells (circles) and whalebone (diamond) reflect minimum sea level and ice-free conditions. Samples in green reflect material redeposited by glacier re-advance from Ringhorndalen (RHD) and Flatøyrdalen (FØD). Note, while the shell at 70 m in Ringhorndalen was resedimented above the contemporaneous sea level by a glacier readvance (black arrow), the whale cranium was also likely resedimented further west and deposited at a lower elevation. Shell ages associated with wave washed terrace landforms are interpreted as sea level indicators (red) and are located at 75 and 45 m a.s.l. Simplistic linear regression projected above limiting marine fauna suggesting the rate of land emergence may have exceeded 2 m per century based on ages of the 75 m and 45 m terraces. Ringhorndalen marine limit indicated by dotted line. Published radiocarbon ages from Ringhorndalen raised marine sediments indicated by grey colored circles (Sharin et al., 2007).

reconstructions suggest that Svalbard fjords reached their peak Holocene warmth during the beginning of the Early Holocene (Salvigsen, 2002; Salvigsen et al., 1992; Hald et al., 2004; Blake, 2006; Farnsworth et al., 2017; Mangerud and Svendsen, 2018). Furthermore, lacustrine proxies indicate summer temperatures also climaxed during this interval in time (van der Bilt et al., 2019; Voldstad et al., 2020). Some of these re-advances have been associated with unsustainable fluctuations related to internal ice dynamics (i.e. not climatically driven positive mass balance; Farnsworth et al., 2017; Farnsworth and Allaart, 2024). However, the persistence of the palaeo-Ringhornbreen margin suggests more factors may contribute to ice-marginal fluctuations than dynamic re-advances driven by a shift in subglacial hydrology, thermal regime, basal conditions, or back stress. While reduced sea ice likely had a significant effect on enhancing regional precipitation, it has remained challenging to constrain this variable and close the budget of the palaeo-mass balance equation (Thomas et al., 2018; Kjellman, 2022; Kjellman et al., 2020).

We constrain three new glacier re-advances to the Late Glacial and Early Holocene. These three ice margins are westerly outlets of the Åsgardfonna ice cap, while previously a Late Glacial-Early Holocene re-advance was described from an easterly outlet into De Geerbukta (Farnsworth et al., 2018). Despite maximum and minimum constraints for these four glacier fluctuations (from the same ice cap), none of the re-advances occur in phase with one another (Figs. 9 and 10). Furthermore, while the Femmilsjøen lake record suggests greatly reduced catchment ice cover by *c.* 10.1 cal ka BP (Allaart et al., 2021a), southerly outlet glaciers in Ringhorndalen and Flatøyrdalen are re-advancing at the same time (Figs. 9 and 10). Given the resolution and uncertainties associated with sub-ice topography, it is possible Longstaffbreen had retreated out of Femmilsjøen by *c.*10.1 cal. ka BP, and meltwater from a persisting (southern) Åsgardfonna was re-routed to other drainages. These data exhibit the intricacies of deglaciation and ice marginal behavior during the Early Holocene. Modeling results suggest some glaciated regions of Svalbard survived the Holocene Thermal Optimum,

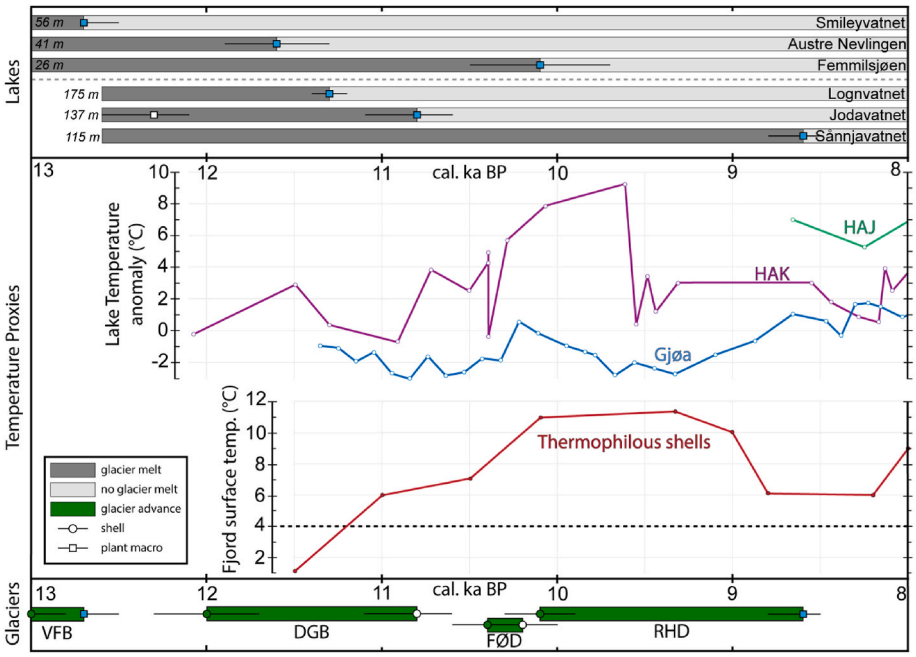

Fig. 9. Wijdefjorden lake records (and their respective elevations) indicating the transition from pro-glacial basins to not receiving glacial meltwater. Lakes ordered by altitude for the Vassfarbukta and Ringhorndalen regions. Alkenone (U^{k}_{37}) based palaeo-temperature anomalies reconstructed from NW Svalbard from lakes Hajeren (HAJ), Hakluytvatnet (HAK) and Gjøavatnet (Gjøa) exhibit variable albeit enhanced warmth during the Early Holocene (van der Bilt et al., 2019). Fjord surface temperature reconstruction derived from shell ages of thermophilous molluscs (Mangerud and Svendsen, 2018). Dotted line represents present day sea surface conditions. Green bars represent the constraint on Late Glacial and Early Holocene re-advances from Åsgardfonna (VFB = Vassfarbukta; DGB = De Geerbukta (Farnsworth et al., 2018); FØD = Flatøyrdalen; RHD = Ringhorndalen). Note that Sånnjavatnet (115 m a.s.l.; unlike Jodavatnet at 137 m a.s.l.) receives meltwater from the Ringhorndalen glacier until *c.* 8.6 cal ka BP (8197–8534), anomalously later than all other lakes and throughout the HTM.

however, the Åsgardfonna ice cap is not highlighted as one of these regions in the minimum distribution of glaciers (Fjeldskaar et al., 2018).

4.3. Glacio-isostatic adjustment and ice dynamics

The paradox of Svalbard's asynchronous re-advances into the warm Late Glacial and Early Holocene challenges our understanding of glacier behavior in response to warming climate (Lønne, 2005; Farnsworth et al., 2018, 2022, Fig. 9). Here we discuss an understudied process that likely played a role in the ice dynamics and the persistence of these outlet glaciers (in addition to enhanced precipitation). The extent to which GIA influences ice dynamics is generally overlooked. This disregard is a result of perceiving the equilibrium line altitude (ELA) as the primary dynamic variable driving glacier-marginal change and overlooking the potential of glacio-isostatically driven terrain modification (Norðdahl and Ingólfsson, 2015). Rate and magnitude of postglacial uplift derived from a relative sea-level curve, is generally understood and widely acknowledged. However, it is often overlooked that postglacial uplift often only accounts for less than half of the total land emergence history. The potential extent of restrained rebound is also now depicted in some glacial and GIA models (Norðdahl and Ingólfsson, 2015; Sbarra et al., 2022). We recognize that enhanced precipitation likely played a role in the sustenance of Early Holocene glaciers (Røthe et al., 2018; Thomas et al., 2018; Kjellman et al., 2020), however, we argue GIA may have also contributed to ice cap mass balance on southern Åsgardfonna. We use the term *rebound effect* to describe the deglacial process of glacio-isostatically driven land emergence influencing mass balance for a given terrain and period. We further argue that the rebound effect likely played a critical role in the persistence of the Ringhorndalen ice margin during the Early Holocene. Here we present a schematic model of this process in hand with our field data. Future efforts should approach modeling these processes under varying terrain and GIA histories.

The southern portion of Åsgardfonna sits almost entirely above 1000 m a.s.l. The hypsometry of the Ringhorndalen tributary glaciers indicate that over two thirds of the present area is located on the highland plateau (Fig. 11). Furthermore, this region is characterized as having the highest ELA for the Svalbard archipelago (>700 m a.s.l.; Hagen et al., 2003). The hypsometry is unique for Svalbard glaciers (Noël et al., 2020) and suggests that while the ELA remains at or below the plateau elevation, the outlet ice margins will remain relatively stable. However, if the ELA rises above the plateau, the outlets will respond considerably. Given our limited knowledge of Late Glacial–Early Holocene ELA in this region (Rea et al., 2020), we will consider it constant and focus on the potential range in GIA driven terrain variation. We assume Late Glacial – Early Holocene ELA was likely equal to or lower than during the LIA maximum and thus minimal ablation was occurring on the top of Åsgardfonna.

We assume ice thicknesses were up to *c.* 2 km over northeast Svalbard during the LGM (Patton et al., 2017; Sejrup et al., 2022), which is widely assumed a minimum for Northern Hemisphere ice sheets during the last glacial (e.g. Lambeck, 1995; Gowan et al., 2021). At equilibrium, such an ice load would displace one third of the underlying landmass below sea level, while two thirds would remain above (Fig. 12A). We can reasonably consider a postglacial emergence and relative sea-level regression on the order of 100 m and use this number in our schematic model for computational ease (Fig. 12B). Raised marine shorelines and postglacial beaches are found up to and exceeding this altitude on Svalbard and other margins of former ice sheets (Forman et al., 2004; Ingólfsson and Norðdahl, 2001; Gowan et al., 2021; Sbarra et al., 2022). We can use relative sea-level curves to infer emergence rates, however, prior to the formation of shorelines (the local deglaciation), we have little constraint on the magnitude (and rate) of emergence, e.g., extent of restrained rebound (Wolcott, 1970; Andrews et al., 1970; Farnsworth et al., 2022, Fig. 12B). Generally, the magnitude and rates of restrained rebound are controlled by ice thickness, ice cover duration and the timing/rate of deglaciation.

Glacio-isostatic adjustment in a continental crust like Svalbard

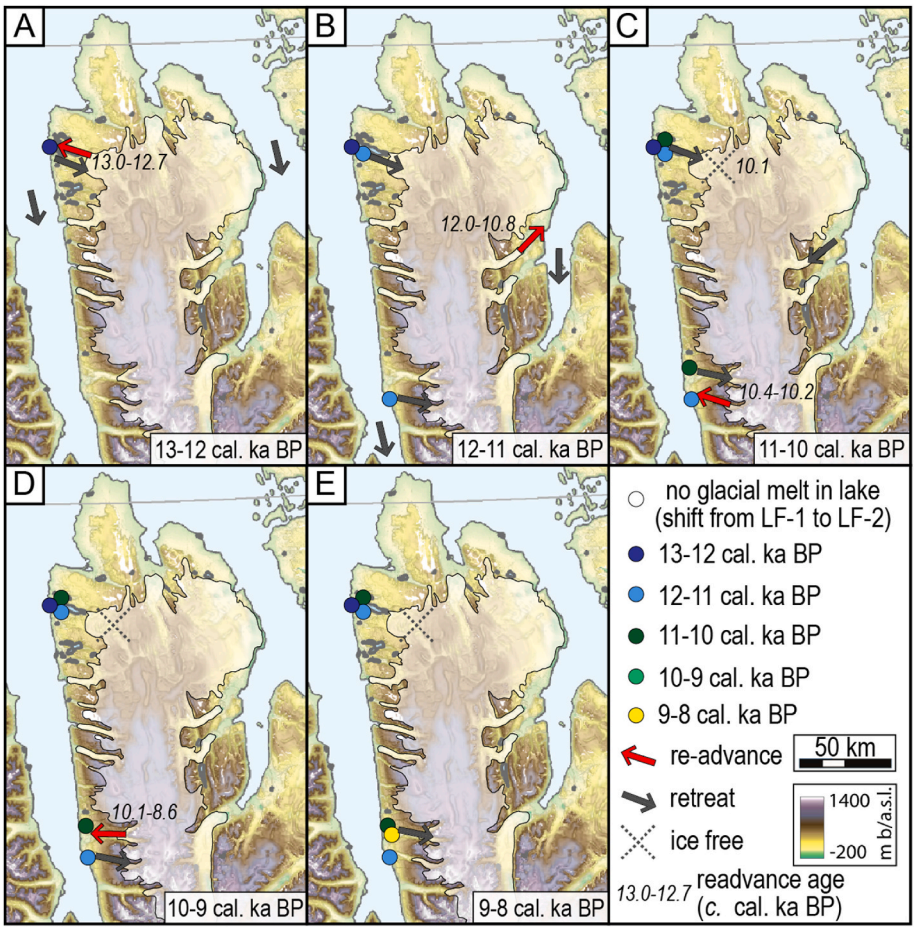

Fig. 10. Digital elevation model and subglacial bed map of NE Spitsbergen presenting sub-ice topography under Åsgardfonna from Fürst et al. (2017). Maps A-E present ice margin fluctuations and proglacial lake conditions in five 1 ka time-slices from 13 to 8 cal. ka BP. Note the range in elevation of the plateau hosting Åsgardfonna ice cap, with the entire southern region extending over 1000 m a.s.l. Color coded proglacial lake records indicate the timing of transition from proglacial to threshold lake basin. Åsgardfonna polygon represents modern extent.

exhibits a half-life of emergence on the order of 2–2.5 ka (Forman et al., 1997; Forman and Ingólfsson, 2000). Thus, Early Holocene land emergence (and relative sea level) responds to Late Glacial deglaciation that occurred several millennia prior (during the Bølling). We do not know if (or assume) glacio-isostatic equilibrium was ever reached (in Svalbard) prior to the deglaciation, and thus we can only estimate the extent of restrained rebound (Fig. 12). Given complete equilibrium, *c.* 600 m emergence occurs prior to deglaciation, resulting in roughly 86% of the total GIA driven land modification (Fig. 12C). Even with 50% of equilibrium (*c.* 300 m emergence prior to deglaciation) and 25% of equilibrium (*c.* 150 m emergence prior to deglaciation), the majority of emergence occurs prior to datable/detectable deglaciation (i.e., before the postglacial period which is accounted for in RSL field data; Fig. 12C). GIA models from North America and Scandinavia suggest vertical bedrock motion exceeded 300 m during the deglaciation, aligning with equilibrium estimates ranging between 50 and 25 % (Pedersen et al., 2021; Godbout et al., 2023). It is fair to assume that full equilibrium was not reached during the last glacial cycle, however 25% of equilibrium is likely an underestimate.

While emergence largely took place after the marine portion of the Svalbard Barents Sea Ice Sheet collapse *c.* 15 ka BP (Brendryen et al., 2020), over half of the emergence had likely occurred prior to the formation of any postglacial shoreline. It is unlikely that the Late Glacial ELA was constant. However, it is plausible that the >1000 m a.s.l. plateau hosting southern Åsgardfonna glacio-isostatically emerged up through the paleo-ELA during the transition from Late Glacial to Early Holocene. Given a postglacial marine limit of nearly 80 m a.s.l., and the low-end equilibrium of 25%, 120 m of emergence would have occurred prior to deglaciation. Furthermore, we show evidence that 30 m of emergence occurs between *c.* 11.6–10.2 cal ka BP (Fig. 8). This 150 m of glacio-isostatically driven land modification is three times greater than the magnitude of reconstructed ELA change from the LIA to 20th century from western Spitsbergen (Røthe et al., 2015).

We acknowledge this process is not planar and differential uplift occurs spatially. In our rudimentary model, we do not account for this variation, but acknowledge that greater emergence likely took place towards Southeast, in the direction of the former center of mass (Forman et al., 2004; Ingólfsson and Landvik, 2013; Hormes et al., 2013). Differential uplift deduced from Early Holocene shoreline gradients measured perpendicular to isobases in coastal Scandinavia suggests uplift variation around 1 m per km (ranging between 1.2 and 0.5 m per km; Svendsen and Mangerud, 1987; Romundset et al., 2018; Regnéll et al., 2023). With this assumption, it is possible that emergence may have varied on the order of tens of meters from northern to southern Åsgardfonna. This dynamic unloading may have resulted in ice divide migration to the southeast across Åsgardfonna during the Late Glacial–Early Holocene (Dugmore and Sugden, 1991).

Given the magnitude of land emergence prior to deglaciation, we suggest rebound effect to be more widely considered with regards to deglacial ice dynamics. Furthermore, it is important to recognize that while rebound effect may have aided the persistence of deglaciating ice sheets during the Late Glacial and Early Holocene, it will have minimal impact on Arctic glaciers and ice caps (except potentially those peripherally to the Greenland Ice Sheet) under current and future

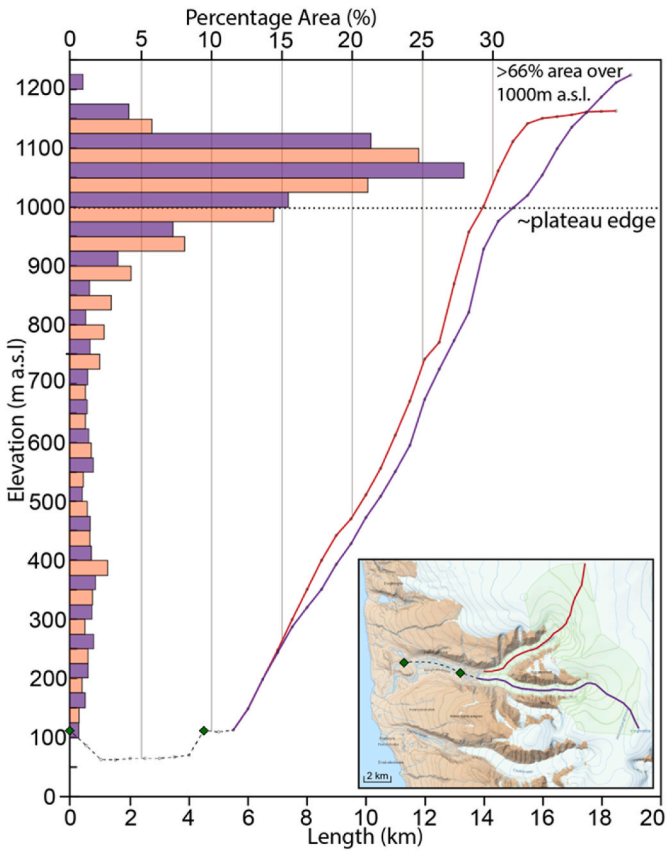

Fig. 11. Glacier profiles and hypsometry of the Ringhorndalen tributary glaciers (purple and red). Note over two thirds of the glacier area is located above 1000 m a.s.l., on the plateau hosting the southern extent of Åsgardfonna (Fig. 1A). The plateau defines a key elevation threshold where changes in (or relative to) ELA will have considerable effect on ice cap extent and dynamics. Glacial profiles and hypsometry were measured on the open access database, GeoSvalbard from the Norwegian Polar Institute.

Northern Hemisphere warming.

5. Conclusions

- We constrain a series of Late Glacial–Early Holocene re-advances from Wijdefjorden tributary valleys hosting outlet glaciers from the ice cap Åsgardfonna, northeast Spitsbergen.
- Despite the dominant perception that Early Holocene tidewater margins retreated inland, we detail a marine terminating ice margin that persisted through nearly the entire Early Holocene, only to be glacio-isostatically uplifted from the fjord.
- The 79 m of postglacial uplift (visible in raised shorelines) likely only reflects a fraction (less than 40 %) of the total emergence that the region experienced since the onset of ice mass loss.
- Glacio-isostatic emergence during and following the regional deglaciation influenced glacier mass balance as the plateau topography was driven up through the palaeo-ELA. We term this deglacial process, *rebound effect.*
- Given this region's high elevation plateau-landscape and the projected restrained rebound, we suggest this upland region of Svalbard likely hosted ice cover throughout the Holocene.
- Rebound effect is not unique to Svalbard. Given the prevalence of tributaries associated with high elevation plateau ice caps and the generally overlooked magnitude of restrained rebound during the deglaciation – we assume the rebound effect likely influenced the margins of other former ice sheets during deglaciation.

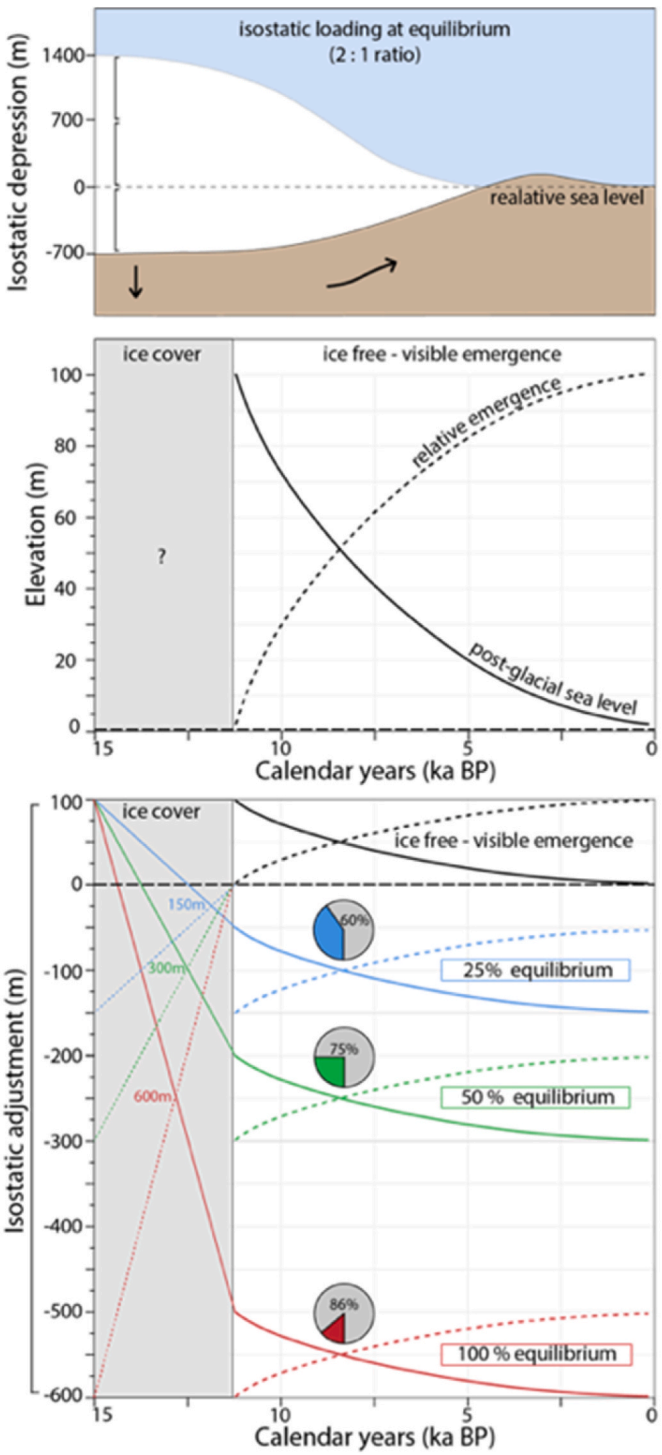

Fig. 12. Introduction and estimates of pre-deglacial emergence or restrained rebound (modified from Farnsworth, 2018). A) Model depicting the distribution ratio of ice sheet situated above to below sea level once isostatic depression reaches equilibrium (modified from Wolcott, 1970; Andrews et al., 1970). B) Schematic relative sea-level curve (solid line) with the inverse relative uplift (dashed line) of 100 m after shorelines became ice-free slightly before 11 ka BP. C) Estimates of the extent of restrained rebound based on an ice sheet thickness of 2100 m and varying levels of isostatic equilibrium.

Declaration of competing interest

The authors declare that they have no known competing financial interests or personal relationships that could have appeared to influence

the work reported in this paper.

Data availability

All data is available or can be made available upon request.

Acknowledgements

This work was supported by The Svalbard Environmental Protection Fund under Grant Project 16/35 to Farnsworth and 17/114 to Allaart. The Arctic Research and Studies program of the Ministries for Foreign Affairs of Norway and Iceland (2017-ARS-79772) supported travel costs to A.S., W.R.F., and S.B. Funding from NERC IRF was granted to Macias-Fauria (NE/L011859/1). We acknowledge The Governor of Svalbard for hut access and Lufttransport for transportation. This manuscript has greatly improved from discussions with Hreggvidur Norðdahl as well as detailed feedback and constructive comments from Anders Romundset and anonymous reviews.

Appendix A. Supplementary data

Supplementary data to this article can be found online at https://doi.org/10.1016/j.quascirev.2024.108625.

References

Alexanderson, H., Henriksen, M., Ryen, H.T., Landvik, J.Y., Peterson, G., 2018. 200 ka of glacial events in NW Svalbard: an emergence cycle facies model and regional correlations. Arktos 4, 1–25. https://doi.org/10.1007/s41063-018-0037-z.

Allaart, L., Müller, J., Schomacker, A., Rydningen, T.A., Håkansson, L., Kjellman, S.E., Mollenhauer, G., Forwick, M., 2020. Late Quaternary glacier and sea-ice history of northern Wijdefjorden, Svalbard. Boreas 49, 417–437.

Allaart, L., Schomacker, A., Larsen, N.K., Nørmark, E., Rydningen, T.A., Farnsworth, W. R., Retelle, M., Brynjólfsson, S., Forwick, M., Kjellman, S.E., 2021a. Glacial history of the Åsgardfonna ice Cap, NE Spitsbergen, since last glaciation. Quat. Sci. Rev. 251, 106717.

Allaart, L., Schomacker, S., Håkansson, L.M., Farnsworth, W.R., Brynjólfsson, S., Grumstad, A., Kjellman, S.E., 2021b. Geomorphology and surficial geology of the Femmilsjøen area, northern Spitsbergen. Geomorphology 382, 107693.

Andrews, J.T., Buckley, J.T., England, J.H., 1970. Late-glacial chronology and glacioisostatic recovery, home bay, east Baffin Island, Canada. Geol. Soc. Am. Bull. 81, 1123–1148.

Bakke, J., Balascio, N., van der Bilt, W.G.M., Bradley, R., D'Andrea, W.J.D., Gjerde, M., et al., 2018. The Island of Amsterdamøya: a key site for studying past climate in the Arctic archipelago of Svalbard. Quat. Sci. Rev. 183, 157–163.

Bartels, M., Titschack, J., Fahl, K., Stein, R., Seidenkrantz, M.S., Hillaire-Marcel, C., et al., 2017. Atlantic water advection vs. glacier dynamics in northern Spitsbergen since early deglaciation. Clim. Past 13, 1717–1749.

Bintanja, R., van der Wiel, K., van der Linden, E.C., Reusen, J., Bogerd, L., Krikken, F., Selten, F.M., 2020. Strong future increases in Arctic precipitation variability linked to poleward moisture transport. Sci. Adv. 6 (7), eaax6869.

Blake, W., 2006. Occurrence of the Mytilus edulis complex on Nordaustlandet, Svalbard: radiocarbon ages and climatic implications. Polar Res. 25, 123–137.

Brendryen, J., Haflidason, H., Yokoyama, Y., Haaga, K.A., Hannisdal, B., 2020. Eurasian ice sheet collapse was a major source of meltwater pulse 1A 14,6000 years ago. Nat. Geosci. 13 (5), 363–368. https://doi.org/10.1038/s41561-020-0567-4.

Briner, J.P., Stewart, H.A.M., Young, N.E., Philipps, W., Losee, S., 2010. Using proglacial threshold lakes to constrain fluctuations of the Jakobshavn Isbræ ice margin, western Greenland, during the Holocene. Quat. Sci. Rev. 29, 3861–3874.

Dallmann, W.K., 2015. Geoscience atlas of svalbard. Norsk Polarinstitutt Rapportserie 148, 1–292.

Detlef, H., O'Regan, M., Stranne, C., Jensen, M.M., Glasius, M., Cronin, T.M., Jakobsson, M., Pearce, C., 2023. Seasonal sea-ice in the Arctic's last ice area during the Early Holocene. Commun Earth Environ 4, 86. https://doi.org/10.1038/s43247-023-00720-w.

Dou, T.F., Pan, S.F., Binjanta, R., Xiao, C.D., 2022. More fre-quent, intense, and extensive rainfall events in a strongly warming Arctic. J. Geophys. Res.: Earth's Future 10, e2021EF002378. https://doi.org/10.1029/2021EF002378.

Dugmore, A.J., Sugden, D.E., 1991. Do the anomalous fluctuations of Solheimajökul reflect ice-divide migration? Boreas 20, 105e111.

Efstathiou, E., Eldevik, T., Arthun, M., Lind, S., 2022. Spatial patterns, mechanisms and predictability of Barents Sea ice change. J. Clim. 35 (10), 2961–2973. https://doi.org/10.1175/JCLI-D-21-0044.1.

Eidesen, P.B., Arnesen, G., Elven, R., Søli, G., 2018. Kartlegging av Ringhorndalen, Wijdefjorden: en uutforsket arktisk oase, Report to the Governor of Svalbard. The University Centre in Svalbard, The University of Oslo. Ecofact Nord AS.

Farnsworth, W.R., Ingólfsson, Ó., Noormets, R., Allaart, L., Alexanderson, H., Henriksen, M., Schomacker, A., 2017. Dynamic Holocene glacial history of St. Jonsfjorden, svalbard. Boreas 46, 585–603.

Farnsworth, W.R., 2018. Holocene glacier history of Svalbard: Retracing the style of (de) glaciation. Department of Geosciences. UiT The Arctic University of Norway, Tromsø, p. 228. Doctoral thesis.

Farnsworth, W.R., Ingólfsson, Ó., Retelle, M., Allaart, L., Håkansson, L., Schomacker, A., 2018. Svalbard glaciers re-advanced during the Pleistocene-Holocene transition. Boreas 47, 1022–1032.

Farnsworth, W.R., Allaart, L., Ingólfsson, Ó., Alexanderson, H., Forwick, M., Noormets, R., Retelle, M., Schomacker, A., 2020a. Holocene glacial history of Svalbard - status, perspectives and challenges. Earth Sci. Rev. 208, 103249.

Farnsworth, W.R., Blake, Jr.W., Guðmundsdóttir, E.R., Ingólfsson, Ó., Kalliokoski, M.H., Larsen, G., Newton, A.J., Óladóttir, B.A., Schomacker, A., 2020b. Ocean-rafted pumice constrains postglacial relative sea-level and supports Holocene ice cap survival. Quat. Sci. Rev. 250, 106654.

Farnsworth, W.R., Ingólfsson, Ó., Mannerfelt, E.S., Kalliokoski, M.H., Guðmundsdóttir, E. R., Retelle, M., et al., 2022. Vedde Ash constrains Younger Dryas glacier re-advance and rapid glacio-isostatic rebound on Svalbard. Quaternary Science Advances 5, 100041.

Farnsworth, W.R., Allaart, L., 2023. Chapter 11 - Holocene glacier landscapes of the Svalbard archipelago. In: European Glacier Landscapes, vol. III. Elsevier 2023. The Holocene.

Fjeldskaar, W., Bondevik, S., Amantov, A., 2018. Glaciers on Svalbard survived the Holocene thermal optimum. Quat. Sci. Rev. 199, 18–29.

Forman, S.L., Ingólfsson, Ó., 2000. Late Weichselian glacial history and postglacial emergence of Phippsøya, Sjuøyane, northern Svalbard: a comparison of modelled and empirical estimates of a glacial rebound hinge line. Boreas 29, 16–25.

Forman, S.L., Weihe, R., Lubinski, D., Tarasov, G., Korsun, S., Matishov, G., 1997. Holocene relative seasea-level history of franz josef land, Russia. Geol. Soc. Am. Bull. 109, 1116–1133.

Forman, S.L., Lubinski, D.J., Ingolfsson, O., Zeeberg, J.J., Snyder, J.A., Siegert, M.J., Matishov, G.G., 2004. A review of postglacial emergence on svalbard, franz josef land and novaya zemlya, northern eurasia. Quat. Sci. Rev. 23, 1391–1434.

Forwick, M., Vorren, T.O., 2009. Late Weichselian and Holocene sedimentary environments and ice rafting in isfjorden, Spitsbergen. Palaeogeogr. Palaeoclimatol. Palaeoecol. 280, 258–274.

Fürst, J.J., Gillet-Chaulet, F., Benham, T.J., Dowdeswell, J.A., Grabiec, M., Navarro, F., Pettersson, R., Moholdt, G., Nuth, C., Sass, B., Aas, K., Fettweis, X., Lang, C., Seehaus, T., Braun, M., 2017. Application of a two-step approach for mapping ice thickness to various glacier types on Svalbard. Cryosphere 11, 2003–2032.

Geyman, E.C., van Pelt, W.J.J., Maloof, A.C., Aas, H.F., Kohler, J., 2022. Historical glacier change on Svalbard predicts doubling of mass loss by 2100. Nature 601, 374–379.

Gjermundsen, E.F., Briner, J.P., Akçar, N., Foros, J., Kubik, P.W., Salvigsen, O., Hormes, A., 2015. Minimal erosion of Arctic alpine topography during late Quaternary glaciation. Nat. Geosci. 8, 789–792.

Godbout, P.-M., Brouard, E., Roy, M., 2023. 1-km resolution rebound surfaces and paleotopography of glaciated North America since the Last Glacial Maximum. Sci. Data 10, 735. https://doi.org/10.1038/s41597-023-02566-5.

Gowan, E.J., Zhang, X., Khosravi, S., Rovere, A., Stocchi, P., Hughes, A.L.C., Gyllencreutz, R., Mangerud, J., Svendsen, J.I., Lohmann, G., 2021. Global ice sheet reconstruction for the past 80000 years. Nat. Commun. 12 (1199) https://doi.org/10.1038/s41467-021-21469-w.

Hagen, J.O., Kohler, J., Melvold, K., Winther, J.-G., 2003. Glaciers in Svalbard: mass balance, runoff and freshwater flux. Polar Res. 22, 145–159.

Hald, M., Ebbesen, H., Forwick, M., Godtliebsen, F., Khomenko, L., Korsun, S., et al., 2004. Holocene paleoceanography and glacial history of the West Spitsbergen area, Euro-Arctic margin. Quat. Sci. Rev. 23, 2075–2088.

Heaton, T.J., Köhler, P., Butzin, M., Bard, E., Reimer, R.W., Austin, W.E.N., Bronk, C.B., Grootes, P.M., Hughen, K.A., Kromer, B., Reimer, P.J., Adkins, J., Burke, A., Cook, M. S., Olsen, J., Skinner, L., 2020. Marine20-the marine radiocarbon age calibration curve (0-55,000 cal BP). Radiocarbon 62, 1–43.

Hogan, K.A., Dowdeswell, J.A., Hillenbrand, C.-D., Ehrmann, W., Noormets, R., Wacker, L., 2017. Subglacial sediment pathways and deglacial chronology of the northern Barents Sea Ice Sheet. Boreas 46, 750–771.

Hole, G.M., Rawson, T., Farnsworth, W.R., Schomacker, A., Ingólfsson, Ó., Macias-Fauria, M., 2021. A driftwood-based record of arctic Sea Ice during the last 500 years from northern svalbard reveals sea ice dynamics in the Arctic Ocean and arctic peripheral seas. J. Geophys. Res.: Oceans 126.

Hormes, A., Gjermundsen, E.F., Rasmussen, T.L., 2013. From mountain top to the deep sea—deglaciation in 4D of the northwestern Barents Sea ice sheet. Quat. Sci. Rev. 75, 78–99.

Hughes, A.L.C., Gyllencreutz, R., Lohne, Ø.S., Mangerud, J., Svendsen, J.I., 2016. The last Eurasian ice sheets – a chronological database and time-slice reconstruction, DATED-1. Boreas 45, 1–45.

Hugonnet, R., McNabb, R., Berthier, E., Menounos, B., Nuth, C., Girod, L., Farinotti, D., Huss, M., Dussaillant, I., Brun, F., Kääb, A., 2021. Accelerated global glacier mass loss in the early twenty-first century, 2021 Apr Nature 592 (7856), 726–731. https://doi.org/10.1038/s41586-021-03436-z. Epub 2021 Apr 28. PMID: 33911269.

Hyvärinen, H., 1970. Flandrian pollen diagrams from Svalbard. Geogr. Ann. 52, 213–222.

Ingólfsson, O., Rögnvaldsson, F., Bergsten, H., Hedenäs, L., Lemdahl, G., Lirio, J.M., Sejrup, H.P., 1995. Late quaternary glacial and environmental history of kongsøya, svalbard. Polar Res. 14, 123–139.

Ingólfsson, Ó., Landvik, J.Y., 2013. The Svalbard-Barents Sea ice sheet: historical, current and future perspectives. Quat. Sci. Rev. 64, 33–60.
Ingólfsson, Ó., Norðdahl, H., 2001. High relative sea level during the bolling interstadial in western Iceland: a reflection of ice-sheet collapse and extremely rapid glacial unloading. Arctic Antarct. Alpine Res. 33 (2), 231–243. https://doi.org/10.1080/15230430.2001.12003426.
Isaksen, K., Nordli, Ø., Ivanov, B., Køltzow, M.A.Ø., Aaboe, S., Gjelten, H.M., Mezghani, A., Eastwood, S., Førland, E., Benestad, R.E., Hanssen-Bauer, I., Brækkan, R., Sviashchennikov, P., Demin, V., Revina, A., Karandasheva, T., 2022. Exceptional warming over the Barents area. Sci. Rep. 12, 9371.
Jang, K., Bayon, G., Vogt, C., Forwick, M., Ahn, Y., Kim, J.-H., Nam, S.-I., 2023. Non-linear response of glacier melting to Holocene warming in Svalbard recorded by sedimentary iron (oxyhydr)oxides. Earth Planet Sci. Lett. 607, 118054.
Jansen, E., Christensen, J.H., Dokken, T., Nisancioglu, K.H., Vinther, B.M., Capron, E., Guo, C., Jensen, M.F., Langen, P.L., Pedersen, R.A., Yang, S., Bentsen, M., Kjær, H.A., Sadatzki, H., Sessford, E., Stendel, M., 2020. Past perspectives on the present era of abrupt Arctic climate change. Nat. Clim. Change 10, 714–721. https://doi.org/10.1038/s41558-020-0860-7.
Kaplan, M.R., Wolfe, A.P., Miller, G.H., 2002. Holocene environmental variability in southern Greenland inferred from lake sediments. Quat. Res. 58, 149–159. https://doi.org/10.1006/qres.2002.2352.
Karlén, W., 1981. Lacustrine sediment studies. A technique to obtain a continous record of Holocene glacier variations. Geografiska Ann. A Phys. Geogr. 63, 273–281. https://doi.org/10.1080/04353676.1981.11880042.
Kjellman, S.E., 2022. Holocene precipitation seasonality on Svalbard and in Northern Fennoscandia reconstructed using organic geochemical and stable isotope proxies. Doctoral Thesis, UiT the Arctic University of Norway, p. 188. https://hdl.handle.net/10037/26641.
Kjellman, S.E., Schomacker, A., Thomas, E.K., Håkansson, L., Duboscq, S., Cluett, A.A., et al., 2020. Holocene precipitation seasonality in northern Svalbard: influence of sea ice and regional ocean surface conditions. Quat. Sci. Rev. 240, 1–15.
Kowalewski, W., Rudowski, S., Zalewski, S.M., 1990. Seismoacoustic studies within wijdefjorden, spitsbergen. Pol. Polar Res. 11, 287–300.
Kylander, M.E., Ampel, L., Wohlfarth, B., Veres, D., 2011. High-resolution XRF core scanning analysis of Les Echets (France) Sedimentary sequence: new insights from chemical proxies. J. Quat. Sci. 26, 109–117.
Lambeck, K., 1995. Constraints on the Late Weichselian ice sheet over the Barents Sea from observations of raised shorelines. Quat. Sci. Rev. 14, 1–16.
Landvik, J.Y., Bondevik, S., Elverhøi, A., Fjeldskaar, W., Mangerud, J., Salvigsen, O., Siegert, M.J., Svendsen, J.I., Vorren, T.O., 1998. The last glacial maximum of Svalbard and the Barents Sea area: ice sheet extent and configuration. Quat. Sci. Rev. 17, 43–75.
Lapointe, F., Retelle, M., Bradley, R.S., Farnsworth, W.R., Støren, E., Cook, T., Rosario, J., 2023. Multi-proxy evidence of unprecedented hydroclimatic change in a high Arctic proglacial lake: linne'vatnet, Svalbard. Arctic Antarct. Alpine Res. 55 (1), 2223403.
Larsen, E.A., Lysså, A., Rubensdotter, L., Farnsworth, W.R., Jensen, M., Nadeau, M.J., Ottesen, D., 2018. Late-glacial and Holocene glacier activity in the van Mijenfjorden area, western Svalbard. Arktos 4, 9. https://doi.org/10.1007/s41063-018-0042-2.
Larsen, N.K., Kjær, K.H., Lecavalier, B., Bjørk, A.A., Colding, S., Huybrechts, P., Jakobsen, K.E., Kjeldsen, K.K., Knudsen, K.L., Odgaard, B.V., Olsen, J., 2015. The response of the southern Greenland ice sheet to the Holocene thermal maximum. Geology 43, 291–294 (2015). 22.
Larsen, N.K., Strunk, A., Levy, L.B., Olsen, J., Bjork, A., Lauridsen, T.L., Jeppesen, E., Davidson, T.A., 2017. Strong altitudinal control on the response of local glaciers to Holocene climate change in southwest Greenland. Quat. Sci. Rev. 168, 69–78.
Lysså, A., Jennings, A., Morigi, C., Stokes, C.R., Winsborrow, M.C.M., 2022. Introduction: processes and palaeo-environmental changes in the arctic from past to present (PalaeoArc) special issue. Arctic Antarct. Alpine Res. 54 (1), 640–647. https://doi.org/10.1080/15230430.2022.2154985.
Lønne, I., 2005. Faint traces of high Arctic glaciations: an early Holocene ice-front fluctuation in Bolterdalen, Svalbard. Boreas 34, 308–323.
Mangerud, J., Svendsen, J.I., 1992. The last interglacial-glacial period on Spitsbergen, Svalbard. Quat. Sci. Rev. 11, 633–664.
Mangerud, J., Dokken, T., Hebbeln, D., Heggen, B., Ingólfsson, Ó., Landvik, J.Y., Mejdahl, V., Svendsen, J.I., Vorren, T.O., 1998. Fluctuations of the svalbard Barents Sea Ice sheet during the last 150 000 years. Quat. Sci. Rev. 17, 11–42.
Mangerud, J., Svendsen, J.I., 2018. The Holocene thermal maximum around svalbard, arctic North Atlantic; molluscs show early and exceptional warmth. Holocene 28, 65–83.
Melvær, Y., 2014a. Kartdata Svalbard 1:100 000 (S100 Kartdata)/Map Data. Norwegian Polar Institute. https://doi.org/10.21334/npolar.2014.645336c7 [Data set].
Melvær, Y., 2014b. Terrengmodell Svalbard (S0 Terrengmodell). Norwegian Polar Institute. https://doi.org/10.21334/npolar.2014.dce53a47 [Data set].
Meredith, M., Sommerkorn, M., Cassotta, S., Derksen, C., Ekaykin, A., Hollowed, A., Kofinas, G., Mackintosh, A., Melbourne-Thomas, J., Muelbert, M.M.C., et al., 2019. Polar regions. In: Pörtner, H.-O., Roberts, D.C., Masson-Delmotte, V., Zhai, P., Tignor, M., Poloczanska, E., Mintenbeck, K., Alegría, A., Nicolai, M., Okem, A., et al. (Eds.), IPCC Special Report on the Ocean and Cryosphere in a Changing Climate. Cambridge University Press, Cambridge, UK and New York, NY, USA, pp. 203–320.
Müller, M., Kelder, T., Palerme, C., 2022. Decline of sea-ice in the Greenland Sea intensifies extreme precipitation over Svalbard. Weather Clim. Extrem. 36, 100437.
Mäusbacher, R., Borgvan der Daug, K.G., Kroemer, E., Müller, J., Wallner, J., 2002. Late Pleistocene and Holocene environmental changes in NW spitsbergen—evidence from lake sediments. Z. Geomorphol. 46, 417–439.
Noël, B., Jakobs, C.L., van Pelt, W.J.J., Lhermitte, S., Wouters, B., Kohler, J., Hagen, J.O., Luks, B., Reijmer, C.H., van der Verg, W.J., van den Broeke, M.R., 2020. Low elevation of Svalbard glaciers drives high mass loss variability. Nat. Commun. 11, 4597. https://doi.org/10.1038/s41467-020-18356-1.
Norðdahl, H., Ingólfsson, O., 2015. Collapse of the Icelandic ice sheet controlled by sea level rise? Arktos 1, 13. https://doi.org/10.1007/s41063-015-0220-x.
Norwegian Polar Institute, 2017. S100 Topographic Raster Data for Svalbard. Norwegian Polar Institute. https://doi.org/10.21334/npolar.1990.44ca8c2a [Data set].
Onarheim, I.H., Årthun, M., 2017. Toward an ice-free Barents Sea. Geophys. Res. Lett. 44–16, 8387–8395.
Ottesen, D., Dowdeswell, J.A., Rise, L., 2005. Submarine landforms and the reconstruction of fast-flowing ice streams within a large Quaternary ice sheet: the 2500-km-long Norwegian-Svalbard margin (57–80 N). Geol. Soc. Am. Bull. 117 (7–8), 1033–1050.
Ottesen, D., Dowdeswell, J.A., Landvik, J., Mienert, J., 2007. Dynamics and retreat of the Late Weichselian ice sheet on Svalbard inferred from high resolution seafloor morphology. Boreas 36, 286–306.
Østby, T.I., Schuler, T.V., Hagen, J.O., Hock, R., Kohler, J., Reijmer, C.H., 2017. Diagnosing the decline in climatic mass balance of glaciers in Svalbard over 1957–2014. Cryosphere 11, 191–215.
Patton, H., Hubbard, A., Andreassen, K., Auriac, A., Whitehouse, P.L., Stroeven, A.P., Shackleton, C., Winsborrow, M.C.M., Heyman, J., Hall, A.M., 2017. Deglaciation of the Eurasian ice sheet complex. Quat. Sci. Rev. 169, 148–172.
Pedersen, V.K., Knutsen, Å.R., Pallisgaard-Olesen, G., Andersen, J.L., Moucha, R., Huismans, R.S., 2021. Widespread glacial erosion on the Scandinavian passive margin. Geology 49, 1004–1008. https://doi.org/10.1130/G48836.1.
Pieńkowski, A.J., Husum, K., Furze, M.F.A., Missana, A.F.J.M., Irvalı, N., Divine, D.V., Trælvik Eilertsen, V., 2022. Revised ΔR values for the Barents Sea and its archipelagos as a pre-requisite for accurate and robust marine based 14C chronologies. Quat. Geochronol. 68, 101244.
Rantanen, M., Karpechko, A.Y., Lipponen, A., Nordling, K., Hyvärinen, O., Ruosteenoja, K., Vihma, T., Laaksonen, A., 2022. The Arctic has warmed nearly four times faster than the globe since 1979. Communications Earth and Environment 3 (1), 168. https://doi.org/10.1038/s43247-022-00498-3.
Rea, B.R., Pellitero, R., Spagnolo, M., Hughes, P., Ivy-Ochs, S., Renssen, H., Ribolini, A., Bakke, J., Lukas, S., Braithwaite, R.J., 2020. Atmospheric circulation over Europe during the younger dryas. Sci. Adv. 6 (2020), 50. https://doi.org/10.1126/sciadv.aba4844.
Regnéll, C., Becher, G.P., Öhrling, C., Greenwood, S.L., Gyllencreutz, R., Blomdin, R., Brendryen, J., Goodfellow, B.W., Mikko, H., Ransed, G., Smith, C., 2023. Ice-dammed lakes and deglaciation history of the Scandinavian Ice Sheet in central Jämtland, Sweden. Quat. Sci. Rev. 314, 108219.
Reimer, P.J., Austin, W.E., Bard, E., Bayliss, A., Blackwell, P.G., Ramsey, C.B., Butzin, M., Cheng, H., Edwards, R.L., Friedrich, M., Grootes, P.M., Guilderson, T.P., Hajdas, I., Heaton, T.J., Hogg, A.G., Hughen, K., Kromer, B., Manning, S.W., Muscheler, R.J., Palmer, G., Pearson, C., van der Plicht, J., Reimer, R.W., Richards, D.A., Scott, E.M., Southon, J.R., Turney, C.S.M., Wacker, L., Adolphi, F., Buntgen, U., Capano, M., Fahrni, S., Fogtmann-Schulz, A., Friedrich, R., Miyake, F., Olsen, J., Reinig, F., Sakamoto, M., Sookdeo, A., Talamo, S., 2020. The IntCal20 northern hemisphere radiocarbon age calibration curve (0-55 cal kBP). Radiocarbon 62, 725–757.
Rubensdotter, L., Rosqvist, G., 2009. Influence of geomorphological setting, fluvial-, glaciofluvial- and mass-movement processes on sedimentation in alpine lakes. Holocene 19, 665–678.
Romundset, A., Lakeman, T.R., Høgaas, F., 2018. Quantifying variable rates of postglacial relative sea level fall from a cluster of 24 isolation basins in southern Norway. Quat. Sci. Rev. 197, 175–192.
Røthe, T.O., Bakke, J., Vasskog, K., Gjerde, M., D'Andrea, W.J., Bradley, R.S., 2015. Arctic Holocene glacier fluctuations reconstructed from lake sediments at Mitrahalvøya, Spitsbergen. Quat. Sci. Rev. 109, 111–125.
Røthe, T.O., Bakke, J., Støren, E.W.N., Bradley, R.S., 2018. Reconstructing Holocene glacier and climate fluctuations from lake sediments in Vårfluesjøen, northern Spitsbergen. Front. Earth Sci. 6, 1–20.
Salvigsen, O., Österholm, H., 1982. Radiocarbon dated raised beaches and glacial history of the northern coast of Spitsbergen, Svalbard. Polar Res. 97, 115.
Salvigsen, O., Forman, S.L., Miller, G.H., 1992. Thermophilous molluscs on Svalbard during the Holocene and their paleoclimatic implications. Polar Res. 11, 1–10.
Salvigsen, O., 2002. Radiocarbon-dated Mytilus edulis and Modiolus modiolus from northern svalbard: climatic implications. Nor. Geogr. Tidsskr. 56, 56–61.
Sbarra, C.M., Briner, J.P., Graham, B.L., Poinar, K., Thomas, E.K., Young, N.E., 2022. Evidence for a more extensive Greenland ice sheet in southwestern Greenland during the last glacial maximum: geosphere, 18 (X), 1–14.
Schomacker, A., Farnsworth, W.R., Ingólfsson, Ó., Allaart, L., Håkansson, L., Retelle, M., Siggaard-Andersen, M.-L., Korsgaard, N.J., Rouillard, A., Kjellman, S.E., 2019. Postglacial relative sea level change and glacier activity in the early and late Holocene: Wahlenbergfjorden, Nordaustlandet, Svalbard. Sci. Rep. 9, 6799.
Sejrup, H.P., Hjelstuen, B.O., Patton, H., Esteves, M., Winsborrow, M., Rasmussen, T.L., Andreassen, K., Hubbard, A., 2022. The role of ocean and atmospheric dynamics in the marine-based collapse of the last Eurasian Ice Sheet. Communications Earth & Environment 3 (1), 119. https://doi.org/10.1038/s43247-022-00447-0.
Sharin, V.V., Alekseev, V.V., Dymov, V.A., Pogodina, I.A., Bol'shiyanov, D.Yu, Gusev, E. A., 2007. New data on the late quaternary stratigraphy and paleogeography of the wijdefjorden region (west Spitsbergen). Doklady Akademii Nauk 412 (5), 822–824. https://doi.org/10.1134/S1028334X07020274.
Skagseth, Ø., Broms, C., Gundersen, K., Hátún, H., Kristiansen, I., Larsen, K.M.H., Mork, K.A., Petursdottir, H., Søiland, H., 2022. Arctic and Atlantic waters in the Norwegian basin, between year variability and potential ecosystem implications. Front. Mar. Sci. 9 https://doi.org/10.3389/fmars.2022.831739.
Stuiver, M., Reimer, P.J., 1993. Radiocarbon 35, 215–230.

Svendsen, J.I., Mangerud, J., 1987. Late Weichselian and Holocene sea-level history for a cross-section of western Norway. J. Quat. Sci. 2 (2), 113e132.
Thomas, E.K., Castañeda, I.S., McKay, N.P., Briner, J.P., Salacup, J.M., Nguyen, K.Q., Schweinsberg, A.D., 2018. A wetter Arctic coincident with hemispheric warming 8,000 years ago. Geophys. Res. Lett. 45 https://doi.org/10.1029/2018GL079517.
Urbański, J., Litwicka, D., 2022. The decline of Svalbard land-fast sea ice extent as a result of climate change. Oceanologia 64, 535–545.
van der Bilt, W.G.M., D'Andrea, W.J., Werner, J.P., Bakke, J., 2019. Early Holocene temperature oscillations exceed amplitude of observed and projected warming in Svalbard lakes. Geophys. Res. Lett. 46 (14,732 14), 741.
van Pelt, W.J.J., Schuler, T.V., Pohjola, V.A., Pettersson, R., 2021. Accelerating future mass loss of Svalbard glaciers from a multi-model ensemble. J. Glaciol. 67 (263), 485–499. https://doi.org/10.1017/jog.2021.2.
Voldstad, L.H., Alsos, I.G., Farnsworth, W.R., Heintzman, P.D., Ha°kansson, L., Kjellman, S.E., et al., 2020. A complete Holocene lake sediment ancient DNA record reveals long-standing high Arctic plant diversity hotspot in northern Svalbard. Quat. Sci. Rev. 234.
Werner, A., 1993. Holocene moraine chronology, Spitsbergen, Svalbard: lichenometric evidence for multiple Neoglacial advances in the Arctic. Holocene 3, 128–137.
Wolcott, R.I., 1970. Isostatic response to loading of the crust in Canada. Can. J. Earth Sci. 7, 716–726.